Partial Grouted Riprap for Enhanced Scour Resistance

Michael Heibaum[1] and Justus Trentmann[2]

[1]BAW-Federal Waterways Engineering and Research Institute, Department of Geotechnical Engineering, P.O. Box 21 02 53, 76187 Karlsruhe, Germany, PH +49 721 9726 3820; email: michael.heibaum@baw.de
[2]Gewatech - Grund- und Wasserbau GmbH & Co KG, Schiefe Güntke 9, 49090 Osnabrück, PH +49 541 121 65-20; email: info@gewatech.de

ABSTRACT

Partially grouted armourstones combine the high resistance against currents and waves of large elements and their flexibility to adapt to ground deformations and the option of installing comparably thin layers. With partial grouting smaller and such often cheaper armourstones can be used to form conglomerates with the same resistance as large armourstones. Grouting can be done in fresh water and in saltwater. Segregation and erosion of the grout when poured or dumped or when fresh grout is loaded by currents and waves is avoided by using special chemical additives or by high speed centrifugal mixing (colloidal mortar) – common anti-wash-out mortar is not applicable. Stone diameters of 10 to 40 cm and a narrow rock size distribution are best for being grouted. To guarantee a successful application of partial grouted armours, a number of tests before, during and after installation have been established for quality assurance.

INTRODUCTION

Scour is a result of the interactions at the boundary of water and soil. In many cases it is considered a hydraulic problem only, looking at it from the water side. So nearly all approaches to assess scour development represent the hydraulic point of view and consider the stability of the top layer, only. But one has also to consider all layers that are influenced by the hydraulic load including the interaction of the surface water and the pore water. On the other hand, sublayers need no consideration if the stability of the top layer is 100 % guaranteed! Such stability can be achieved by grouting the top layer to keep the armour material in place even under high hydraulic actions.

An important parameter for designing a scour protection is the surface geometry of the protected area. Shallow beaches and banks are much less susceptible to scouring than steep banks or structures like breakwaters and dikes with steep slopes. The stability of armour elements decreases with an increase ot the inclination of the surface. Since often surface geometry cannot be modified to the desired shape, solutions have to be sought to stabilize the armour without increasing their size to unproportional dimensions, e.g. grouting the top layer.

Partial grouting (Fig.1) is a reliable and well established method to meet the requirements for a long lasting scour protection including sufficient permeability to avoid excess water pressure below the armour. With this method, the stability of the traditional armour made of loose elements is increased to a very large extent. Partial grouting means filling the voids of a riprap layer to 35 - 50% with a special mortar, thus creating an armour layer with high resistance, (still) high permeability and sufficient flexibility. Generally partial grouting of armour stones is used if the stability of armourstones is not sufficient due to the magnitude of the hydrodynamic action (waves, turbulent flow) and because of the weight of the armourstones, thickness of the armour layer and slope inclination.

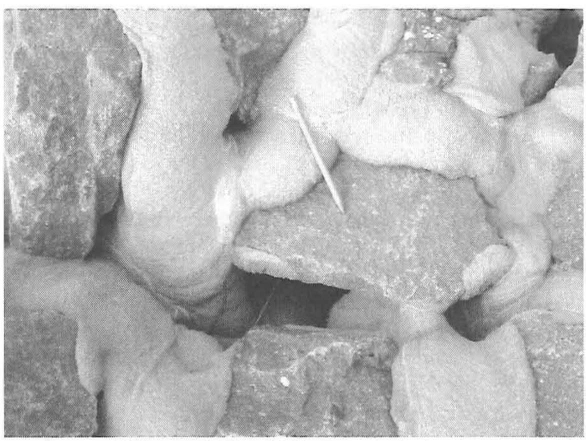

Figure 1. Partially grouted riprap

ARMOUR LAYER

General

An armour layer to prevent scouring may be permeable or impermeable. If impermeable systems are used, the development of excess pore water pressure below the layer should be ruled out. Excess pore water pressure or uplift pressure often is one of the reasons for damage of the armour layer or even the whole system. A steady excess pore water pressure (uplift pressure) may be caused by a high groundwater table compared to the level of the surface water. An unsteady excess pore water pressure below the cover layer develops when there is a rapid lowering of the surface water level, for instance due to waves or a ship induced drawdown. But even in the subsoil below permeable cover layers an excess pore water pressure may develop, however to a lesser extent. Since natural water is not an ideal (incompressible) fluid, the pore water pressure will lag the surface water pressure change. The length of this time delay depends on the permeability and the saturation of the subsoil.

At the coast, impermeable protection is used in many places. The top layer in most cases is fully grouted riprap, using bituminous or concrete grout. Sometimes a lining of asphaltic concrete, cast asphalt or cement bonded material is installed. Also geosynthetic mattresses with concrete fill are used. To avoid the development of excess water pressure, often a permeable cover layer is recommended for scour countermeasures. At first sight, a permeable cover layer seems to ask for more effort and costs compared to an impermeable one. A filter is always needed and the placement of the top layer material has to be done much more accurately, but in the end such a system is more successful in most cases.

Flexibility (serviceability)

Besides the problem of excess water pressure below the lining, a second problem occurs with impervious armour layers, namely suberosion of the soil from below the lining. Only in ponds and narrow rivers can the lining be placed from one side of the water to the other. So the toe of the armour layer of coastal protection and protection of wider rivers is a critical point. The soil may be washed out from under the layer, initiating regressive erosion and resulting in large voids. This is even intensified by the fact that all the impervious armour layers are rather rigid – even the bituminous systems. Due to these boundary conditions, erosion can occur over a long time without being detected, since the strength of the armour is high enough to bridge the voids, but finally a large collapse occurs (Fig. 2).

Figure 2. Failed concrete mattress lining

Scouring is a dynamic geomorphic process that can be stopped completely only with major effort. Scouring at the borders of scour protection is inevitable but it can be accepted to a certain extent, if the protection system is chosen appropriately, hence resulting in a major requirement: a good scour protection system has to be flexible. The demand for flexibility holds for all elements of scour repair and prevention work, i.e. fill, filter and armour. The best measure possible will be implemented when all layers adapt to the geometry given and are able to follow a changing geometry due to hydrodynamic processes. Secondary scouring at the edges of a scour protection layer is nearly inevitable, since the transition from an artificial to a natural bed always causes local erosion. So only a flexible protection layer guarantees the adaptation to the newly developing geometry until an equilibrium is reached. (Another option would be to bury the toe to a sufficient, i.e. rather great, depth.)

Armour elements

To meet the above mentioned requirements of permeability and flexibility, the armour for a scour countermeasure is built from single elements that may be placed randomly or regularly, mutually connected or loose.

Armourstones or riprap is maybe the most often used material for protection systems to stop or to reduce scouring or to rehabilitate existing scour holes. Solutions at reasonable costs can be attained if this material is sufficiently available. Sometimes riprap is considered a temporary countermeasure only, an opinion which may originate from the use of stones that are too small or from armour layers without a filter beneath.

Concrete elements are used when natural material is not available to the necessary extent. The production costs are much higher but their use is justified if the transportation distance of rock is too large. In certain cases it may be beneficial to produce the elements on-site. There is a large variety of concrete elements that are used as an armour layer. They will not be listed here in detail, but there are three groups to be mentioned: Elements of many different shapes that are used like riprap, blocks that are placed regularly ("paved") and elements that are mutually connected.

Stability of armour elements

The resistance of all single elements against hydrodynamic forces increases with the weight of the element. But increasing the weight, which is usually linked with an increasing diameter, means increasing the layer thickness, too. And since the voids between larger elements also become larger, the elements of the layer below (filter or cushion layer) have to be larger to ensure their not being eroded through the cover layer. Maybe even an additional layer is necessary. But an increasing layer thickness may be incompatible with the geometry requirements.

To limit the thickness of the armour layer but to provide a comparable resistance against the erosive forces of currents and waves, cover layers with mutually connected elements can be fabricated. The general idea is to use smaller and often cheaper elements, but simultaneously to gain high resistance against the hydraulic load by connecting them to larger elements, to "mattresses" or to continuous layers. Examples of permeable continuous layers are open stone asphalt, mutually interlocking or cable connected concrete elements, stone mattresses etc.

A paved cover layer (natural stones or concrete blocks) also shows an increased resistance against hydraulic loads while remaining limited in thickness.

But the high resistance is lost if only one element is missing and the permeability is limited since one element is placed very close to the next.

The use of gabions is a well known method to achieve large elements with only small voids. Gabions are made of riprap or even smaller stones filled in a wire mesh basket. They are very versatile elements concerning the shape of the single element as well as the shape of the whole cover layer. Gabions may be prefabricated or - in the dry only - filled in place.

Stone mattresses are similar to gabions and manufactured like these. They are usually thinner than gabions, but cover a larger area. If placed in the dry, they can be connected to each other thus creating a continuous armour layer. Mattresses are prefabricated when they are placed in the wet, but up to a few square metres only due to the weight.

Cable connected systems are similar to stone mattresses, and like mattresses, their size is limited when placed in the wet. In the dry they can be assembled continuously, depending on the system.

Open stone asphalt is a very well known continuous cover layer in coastal protection, but can be placed only in the dry. In the wet prefabricated mattresses of open stone asphalt are used.

Continuous layers also may be created by so called geosynthetic mattresses filled with concrete or mortar. They can be placed continuously with the fabric sewn together as needed and then filling the mattress. Mattresses of uniform thickness would be inflexible and impermeable. To achieve a certain flexibility and permeability, mattresses consisting of columns and rows of "pillows" are used – like mutually connected bags. The seams between the concrete filled pillows provide the necessary permeability of the layer and the desired flexibility for good adjustment to any deformation of the subsoil.

All cable connected systems, gabions and stone mattresses are endangered by corrosion and abrasion of the cables or the wire mesh, so the long term stability of both steel and polymer wires is limited. Abrasion is due to sediment transport or due to the relative movement of wire or cable and armour element. Gabions and stone mattresses cannot be filled so tightly that the stones do not agitate at all under the hydraulic load.

Partial grouting allows for both, creating larger elements or a layer of mutually connected elements of minor thickness. Conglomerate-like larger elements (Fig. 3) are similar to gabions. But also a continuous layer may be created by spreading the grout in an appropriate manner.

Grouting has proved its long term stability and its ability to keep the costs low. Laboratory tests at the Braunschweig University, Germany, proved stability up to a flow velocity of 8 m/s (test report unpublished). Since the riprap is dumped or placed as needed and only then the layer is grouted, any shape of the cover layer may be obtained. Thus a close contact to structural elements like piers, piles or walls can be achieved.

GROUTING

General

With full grouting the voids between the armourstones are filled with grouting material completely. With partial grouting only parts of the voids between the armourstones are filled with grout. Grouting materials are liquid during installation and solidify after a certain hardening period. This period depends on the type of material. Cement bonded grouting materials are made of cement, aggregates and water as well as optional additives. Bituminous grouting materials are made of bitumen, sand and filler (grain size < 0.09 mm). The only bitumen bonded grouting material considered applicable for impermeable grouting is asphaltic mastic. Grouting can be done in fresh water and in saltwater.

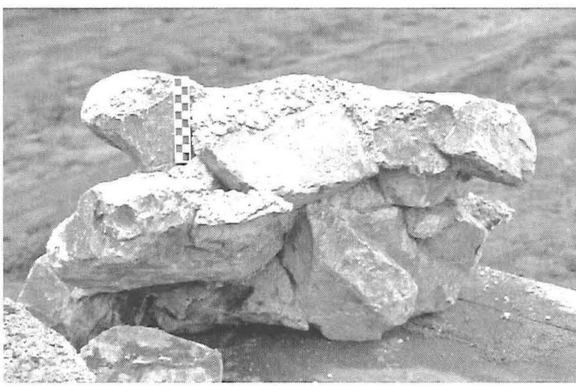

Figure 3. Conglomerate of grouted riprap

Partial grouting is done line by line or spot by spot, the latter resulting in conglomerate-like elements while the former results in a continuous layer. With the correct amount and the correct distribution of the grout the armour layer still remains flexible to follow the ground deformation.

To stabilize the position of the armourstones, generally it is sufficient to fix the stones on the surface of the armour layer. In case of high wave loads or strong turbulent flow (e.g. propeller wash, flow over weirs) an armour layer must be grouted in such a manner that every stone is fixed against lift forces. Consequently, the grouting material must be distributed over the entire cross section of the armour layer. Usually less than 50 % of the voids are filled with grout. A permeability of more than 1×10^{-3} m/s should be guaranteed.

With increasing hydrodynamic effects on the armour layer the grouting material quantities as well as the grouting depth must increase. To achieve a sufficient bonding effect as well as simultaneously a sufficient water permeability of the armour layer, great care has to be taken that the distribution of grouting material in the armour layer meets the requirements.

For stability reasons the water permeability of the armour layer on permeable ground must be larger than the permeability of the underlying filter. Based on experience, this criterion is fulfilled in most cases if the remaining void ratio is not less then 10 % in any layer or volume.

Armourstone requirements

The requirements for armourstones used in revetments are laid down in the European Standard EN 13383-1 which specifies various standard size classes. Small armourstones are defined by the sieve perforation size, D, (size of the square perforations) and are referred to as class $CP_{x/y}$ (Coarse Particle, x being the lower class boundary [mm] and y the upper class boundary [mm]). The larger classes are defined by the weight, G, of the stones as light gradings $LM_{x/y}$ (Light Mass, x = lower class boundary [kg], y = upper class boundary [kg]) or heavy gradings $HM_{x/y}$ (Heavy Mass).

The size class $CP_{90/250}$ with a mean diameter of D_{50} = 150 mm is recommended for the construction of partially grouted cover layers. The proportion of fines in the size class must be limited by specifying 90 mm as the minimum value of D_5 in order to ensure a sufficiently large void size. Stones of class $LMB_{5/40}$ (mean weight G_{50} = 14 kg) may also be used. Generally, the void size distribution should be even, which is achieved by narrowly graded riprap.

Qualified placing of the armourstones is essential for a successful installation of partial grouted armour layers. Placing under water usually is done mechanically by special equipment (dumping pontoons). No additional grading or pushing down by an excavator shovel or else should be done.

Grout requirements

Cement bonded grouting materials are recommended for partial grouting. Cement grouting "glues" one stone to the next, while asphalt grouting only forms a "clamp" to hold the single stone in place. Therefore bituminous grouting materials (asphalt) are not further dealt with.

There are a number of requirements for grouting material to be met for successful application:

- The basic materials need to match a building material standard or to have the valid registration mark of an approved testing laboratory.
- The basic materials need to pass a quality control.
- The grouting material must be harmless towards environment. (Cement bonded grouting materials are harmless towards environment if approved constituent materials are used.)
- The grouting material must have a long-term resistance.

The grouting material in fresh condition must be in such a liquid stage that the voids of a riprap layer are filled in the requested manner. The flow characteristic of cement bonded grouting material is different when being installed under water or in the dry. Consequently testing results of installation in the dry do not apply to installation under water.

Fresh grout needs high resistance to erosion, i.e. the grout must not segregate when poured through water or dumped. This holds always when installed under water and for the installation in the dry, if currents and wave actions are possible on the freshly grouted layer (e.g. tide region). Standard cement bonded grouting materials only have a high resistance to erosion if they are combined with suitable chemical additives. A high resistance to erosion is also established through the preparation of a cement bonded grouting material in a colloidal mill with high velocity shear action (2200 – 2500 U/min). Common anti-wash-out mortar is not applicable.

High resistance to frost is required if the grouted layer is installed in a zone of fluctuating water level up to 1m under the lowest local water level and in the high water level zone.

The consistency of the grout should be such that the amount of fill is never filling the voids too much and decreasing from top to bottom. If the consistency is too low, the grout will flow through the armourstones and clog the filter. If the consistency is too high, only the top voids will be filled, leading to an insufficient permeability. The system and the grout chosen have to prove their ability by tests, since the grout behaves different in the dry and under water. Usually test boxes with a base of at least 3 m^2 are installed under water, filled with armour layer material and lifted again after being grouted to check the result (Fig. 4). The grout distribution should be as desired and the bond strength of a single stone should be above 2 kN per stone.

Figure 4. Test box to check grout distribution and/or permeability

Installation

Installation should be done only by a qualified contractor and skilled and well trained workers. Placement of grout below the water table needs either divers (for small areas and narrow spaces) or special machines. Only to a water depth of 1 m it can be done by hand from above the water table. The tremie method is not applicable for partial grouting.

The armourstones must have a clean surface in order to achieve the desired results of bond strength with the grouting material. Consequently, the grouting work must be done immediately after installation of the armourstones. If sediments are left behind from floods or construction procedures the dirty armourstones must be cleaned and the voids must be free of any debris. If there is doubt concerning the quality of the cleanliness, the bond strength must be tested.

Cement bonded materials installed in the dry must follow the guidelines for the curing of concrete and therefore must be kept moist especially when exposed to high temperature and sunlight.

Frozen armourstones are unfavourable for grouting.

TESTS

Resistance to erosion

In order to test the resistance to erosion according to the "washing out method", the grouting material is placed in screened basket, which is then dropped three times through a water tank of 1 m height (Fig. 5).

The test procedure is as follows: 2000 g of the grouting material is filled into a screened basket (mesh width of the sieve 3 mm) and is then compressed by tamping it lightly. The screened basket is then dropped through the 1 m high water column in the test cylinder in free fall. Afterwards the basket is raised. This procedure is repeated two times. Then the loss of mass of the grouting material is determined, with a permissible loss of mass < 6%.

Figure 5. Test apparatus for the washing out method

Grouting material quantities and distribution

A test cylinder or box is filled with armourstones to the required layer thickness (Fig. 4). First the weight of the empty test cylinder is determined, then the total weight followed by determining stepwise the weight differences of the test cylinder when dipping it into water in 5 cm steps. The void ratio of the rock fill for different steps is calculated from these weight differences. The armourstones in the test box are grouted according to the construction method. After the solidification of the grout, the immersion weighing of the test box is repeated using the same steps as before. Based on the comparison of the weight of the respective immersion depths the void volume filled with grout or the remaining void ratio is calculated from the known dry density of the grouting material.

Water permeability

The testing of the water permeability (k-value) of partially grouted armour layer is performed on at least 2 test samples. This test is done with a special test apparatus similar to the one used for the determination of the grout distribution according to the principle of falling hydraulic head.

Bond strength

In order to test the bond strength of grouted armour layers at least 5 non-neighbouring stones of the top rock layer must be supplied with an anchor bolt. After solidification the tensile force is measured when pulling the stone from the grouted layer.

CONCLUSION

A protection system suitable as scour countermeasure should be permeable to avoid excess water pressure below the armour layer. Furthermore it has to meet the following requirements:

- being flexible so as to be able to follow soil deformations and further scouring at the edges,
- incorporating a filter to avoid winnowing or contact erosion,
- having sufficient resistance against the hydraulic loads.

There are a lot of systems available for armour layers. Among them partially grouted riprap has proved to perform extremely well, since it combines the high resistance against currents and waves of large elements and their flexibility to adapt to ground deformations with the possibility of building comparably thin layers. With partial grouting smaller and such often cheaper armourstones can be used to form conglomerates with the same resistance as large armourstones. And partial grouting allows a tight connection to other structural elements since often these contact zones are the origin of progressive scour. To guarantee a successful application of partial grouted armours, a number of tests before, during and after installation have to be passed for quality assurance.

REFERENCE

EN 13383-1: Armourstone – Part 1: Specification (2002-05)

Scour at Offshore Structures

R.J.S. Whitehouse[1], J.M. Harris[1], M.ASCE, T.R. Mundon [2] and J. Sutherland[1]

[1]HR Wallingford, Howbery Park, Wallingford, Oxfordshire, OX10 8BA, UK; +44 (0)1491 835381; email: r.whitehouse@hrwallingford.co.uk; j.harris@hrwallingford.co.uk; j.sutherland@hrwallingford.co.uk
[2]HR Wallingford Inc, 3100 Timmons Lane, Suite 435, Houston, TX, 77027, USA; email: t.mundon@hrwallingford.co.uk

ABSTRACT

The drive for marine offshore renewables developments has led to focussed requirements for scour hazard assessment relating to foundations and the cabling necessary for in-field transmission and power export. Foundations can represent a significant proportion of the installed capital costs of a renewable energy device so the offshore renewable energy community can benefit from the sharing of information and the development of common approaches to scour and geotechnical issues. Foundation options including monopiles, multi-piled tripods and jackets, gravity bases, or suction piles are being considered for a variety of offshore renewable installations. This paper concentrates on scour assessment challenges in currents and waves, including scour experience at built foundations, time-series predictions of scour and considerations with respect to the evaluation of heterogeneous soils.

INTRODUCTION

In January 2007, the European Commission published a Renewable Energy Roadmap outlining a long-term strategy that called for a mandatory target of a 20% share of renewable energies in the European Union's (EU) energy mix by 2020. The target was endorsed by EU leaders in March 2007. To achieve this objective, the EU adopted a new Renewables Directive in April 2009, which set individual targets for each member state. There are a number of technologies that are classed as renewable including wind, hydro-power, tidal and wave.

To date within the United Kingdom (UK) a number of demonstrator projects have been constructed covering wind, wave and tidal generation. However, only offshore wind has been developed at large-scale at present as part of two rounds of commercial development of offshore wind farms (OWFs). In June 2008, The Crown Estate – responsible for licensing seabed use – announced proposals for a third round of offshore wind farms to develop an additional 25 GW of energy to the 8 GW already planned for under Rounds 1 and 2. The size of these Round 3 developments will vary, but the largest of these zones will involve the construction of around 2500 seabed foundation structures.

Under Round 1 and 2 developments only monopile foundations have been used, primarily due to cost and being tried technology, although several other European (non UK) wind farms have been built using gravity base foundations. Byrne and Houlsby (2003) state that "in contrast to typical oil and gas structures used offshore, for a wind turbine the foundations may account for up to 35% of the installed cost". Therefore, one of the future challenges for large volume installation of offshore wind is the control and minimisation of these costs.

For tidal energy devices one of the principal requirements for many of the devices proposed is their placement in areas of strong tidal energy, and this has implications not only for the stability of the foundation option, but also for the construction methodology.

Similarly wave energy devices are designed to be located in shallow, coastal environments as either floating or bottom mounted systems. These devices, by design, are intended to be located in environments with strong wave action. This may be substantial during storm events, which has implications for the integrity of the anchoring system keeping the wave device on station or the design of the device if it is seabed mounted.

This paper explores some of the challenges facing the offshore renewable industry in respect of the foundation designs and specifically the requirements for scour hazard assessment using the combined experience from those developments currently operational or under construction.

PRELIMINARY ASSESSMENT OF SCOUR HAZARD

At its simplest, an assessment of the scour risk at any given site can be based on observing natural features in the seabed environment that indicate the sediment has been mobile in the case of sands, or eroded, in the case of clays (Table 1). This assessment does not provide any information about when the seabed soil was mobilised but it does indicate whether the site is likely to experience soil mobility. In this situation, where the soil is mobile under the prevailing environmental conditions, the installation of a structure on the seabed can induce scouring.

Table 1. Examples of seabed features indicating mobility or erosion

Sand – indicators of mobility	Clay – indicators of erosion
Ripple marks	Longitudinal furrows or grooves
Megaripples	Obstacle marks – scour around rocks or other debris on the seafloor
Sandwaves	
Obstacle marks – scour and deposition around rocks or other debris on the seafloor	

It may also be necessary to consider bed changes due to the movement of sandbanks, sandwaves, ridges and channels. These changes, which can be progressive, seasonal, or caused by extreme events, lead to variations in seabed level and composition of the soil.

The next level of assessment combines the known characteristics of the hydrodynamic conditions (wave and currents) with knowledge of the soil to make an assessment of the soil mobility status (Whitehouse, 2006). This leads to an understanding under what conditions the soil is mobile and feeds directly into the scour assessment methodology. Therefore, the soil characterisation is an important aspect of the assessment methodology.

MARINE SOILS

Critical to any foundation design are geotechnical considerations. Scour in the marine environment is a physical process related to the movement of seabed sediment by the flow of water away from a structure. The soil conditions are described by geotechnical parameters, therefore, scour is of a geotechnical nature as it relates to the reduction in ground level around a structure. Scour in uniform cohesionless soils is relatively well understood, but marine soils are rarely uniform in structure and can be multi-modal in their grading as well as exhibiting a varying amount of cohesion. Assessing the extent of the scouring in these real soils is far more complex and the methods available more limited.

The Earth Materials approach developed by Annandale (2006) defined a stream power parameter, P, which is related to the rate of flow energy dissipation and an erodibility index, K, which is related to the erodibility of the bed material. If $P < K$, no erosion takes place, but if $P > K$, erosion will occur. The Erodibility Index was defined for earth materials ranging from cohesionless granular soil through to massive hard rock, and including weathered rock. The approach allows for the physical properties of the soil to be considered and although the method does not directly take into account the chemical properties of the material, the mass strength number, M_S, represents the relative influence of chemical bonding properties of the soil through the unconfined compressive strength.

Whether a site with clay layers will experience significant scour could be addressed using observations at existing structures, although this is not possible at a new site, through direct testing of erosion resistance performed in parallel with site investigation activities, by monitoring of scour around foundations once installed, or, for example, with application of the Earth Materials approach. Figure 1 shows an example application of the latter to a site in 30 m of water where clay underlies the whole site to depth. Over parts of the seabed there is a veneer of sand and gravel, generally to a depth of several decimetres, which is expected to scour due to the prevailing hydrodynamic conditions: Peak tidal currents in the water column vary between 0.7 and 1.7 m/s. Significant wave heights of up to 3.6 m were recorded, with a maximum wave height of 6.2 m.

Figure 1 shows the variation with depth in the bed of the required stream power for erosion of an intact soil sample, with inputs derived directly from site investigation, and a remoulded sample. The curves of available stream power – in increasing order – relate to waves alone, currents alone and combined waves and currents showing the profile with depth if a scour hole was formed. Whilst in this particular case neither soil profile is predicted to scour given the available hydrodynamic conditions, the effect of remoulding reduces the soil strength significantly and thereby reduces the required stream power to erode the sediment by around 50% on average. This could have important implications for sites where the soils are likely to be significantly impacted on by installation of the foundation or other construction processes, for example, by dredging. In addition, other effects may occur, for example, the observations (2004) at Kentish Flats OWF (another predominantly clay site) indicate a depression forms around the installed foundation; this was probably due to the combined effect of soil deformation during piling (a geotechnical issue) and scour (a hydraulic issue).

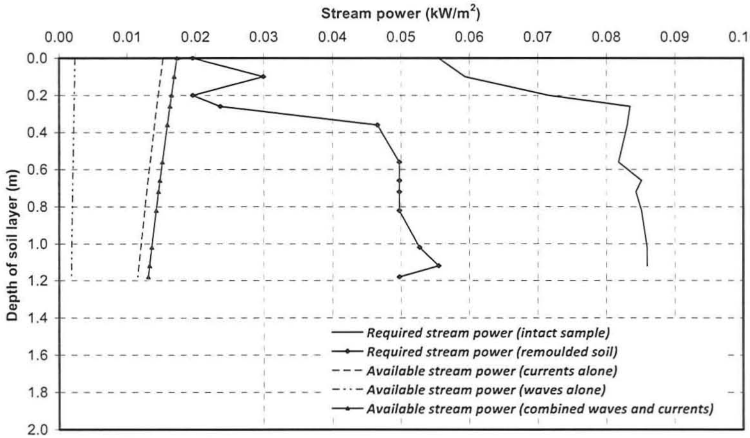

Figure 1. Plot showing the application of the Earth Materials to an offshore wind farm site with predominantly clay marine soils.

Additional impacts can arise from the operation of vessels during installation. Also observable in the monitoring surveys at Kentish Flats OWF were regular depressions caused by the jack-up vessel at the time of installation of the foundations. Immediately post-construction these depressions were recorded to have depths of between 0.5 m and 2.0 m. At the time of the survey in late 2007 these depressions had reduced, on average, by 0.6 m.

TIME-SCALE OF SCOUR DEVELOPMENT

Scour development under waves and currents around offshore structures is a time varying process. Whether a scour hole will continue to develop, remain at some equilibrium or fill in is a function of the hydrodynamic processes existing at any given time. Therefore, scour development is analogous to the growth and decay of, for example, seabed ripples. Under tidal flows the current reverses direction with the tidal state, consequently the scour development will take place in two directions. In addition, the magnitude of the current will vary through the period of the spring-neap tidal cycle.

Whitehouse (2006) highlighted the need to develop time-series methods for scour development and, in particular, using the results from such methods to investigate the probability of exceedance of scour around the foundations of offshore structures. This is a clear way of communicating the likelihood of scour occurring to particular depths from which risks to a particular project can be evaluated.

The time variation with respect to the period between installation of the foundation structure and the monitoring survey or surveys is important as there will be a general increase in scour depth to some equilibrium condition over a time-frame that will vary with site conditions. Under steady flow conditions the scour process will take some time to develop a scour hole and the development is often defined by a negative exponential growth curve (Whitehouse, 1998).

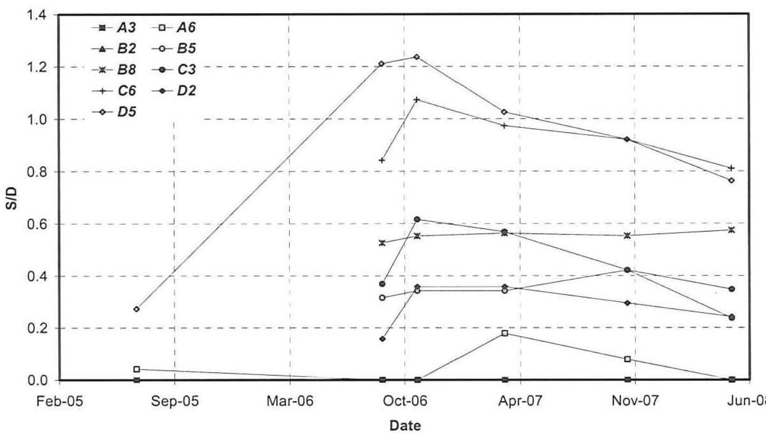

Figure 2. Variation of non-dimensional scour depth with time at Barrow Offshore Wind Farm (COWRIE, 2010).

The monitoring data for Barrow indicates a general growth in scour (Figure 2), although some deeper values have reduced more recently. Caution should be taken though in inferring a general reduction in scour depth with time, as this may just be a function of the prevailing conditions at the time of the survey rather than a general trend. A clearer picture of time evolution will be obtained from carrying out surveys at short time intervals after installation. Recent studies by Harris *et al.* (2010) suggest that the scour depth can vary significantly under combined current and wave conditions through time as demonstrated in Figure 3.

Harris *et al.* (2010) developed a semi-empirical based model to predict the time-evolution of scour. Figure 3 shows the results from the model at prototype scale using a pile diameter typical of that used in offshore wind farm construction (4 m diameter). At this site there was a moderate water depth (≈ 8 m mean sea level) and the results indicate a clear difference between the scour predicted including waves and not including them, and without waves there is more of a tidal effect evident in the scour depth evolution – the increased amplitude of oscillation relates to periods with larger tidal range and storm driven currents. The peak scour depth achieved under both scenarios is less than the maximum assumed equilibrium scour depth ($1.3D \approx 6.1$m) and this indicates that at this location there is still a slight modification to the scour depth as a result of pile diameter to water depth ratio. There is also a significant difference between the initial rate of growth of scour with and without waves at this location with a much smaller initial rate of scour when waves are present. Validation of this kind of detailed modelling requires continuous time-series data of environmental conditions and scour depths at the foundation.

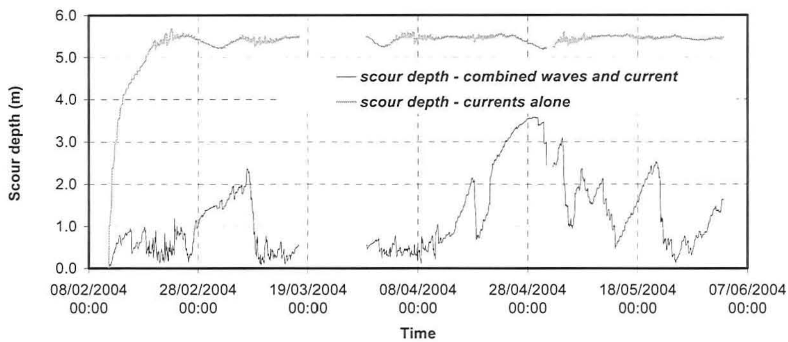

Figure 3. Modelled variation of foundation scour depth at a moderate water depth site (Harris *et al.*, 2010).

EVIDENCE BASE

It is considered good practice for scour evaluation that during the design process of the foundation an appropriate analysis is made for local scour arising from the influence of waves and currents taking account of spring and neap conditions and the influence of storm events, as well as the relative magnitude of waves and currents which will vary from location to location. In those locations where a strong reversing tidal flow exists it is advisable to evaluate the influence of that current pattern on scour development. The potential for scour interaction between adjacent foundations needs to be assessed. Finally, the influence of variations in bed level over the design life of the wind farm needs to be considered; this may arise from regional changes or local changes due to migration of seabed features such as banks, sandwaves or channels.

Studies carried out for Round 1 and 2 developments (DECC 2008; COWRIE 2010) have drawn together the sediment process monitoring work carried out on Round 1 and 2 offshore wind farm developments. They have reviewed the methods, data, results and impacts in order to identify lessons learnt and to provide relevant recommendations for future developments, whilst establishing an accessible evidence base. Results of this evaluation were presented by Whitehouse *et al.* (2008).

As part of these studies those aspects of sediment monitoring related to scouring around wind turbine foundations have been evaluated with the aim of examining scour patterns and lessons learnt at OWF sites in UK and European waters, where sufficient data is available. The evidence database on scour relates to monopile foundations in different sediment and hydrodynamic environments based on site surveys. The new insights from this data – based on work by the authors for COWRIE (2010) – are discussed with data presented in the standard parameters of the scour depth (S) non-dimensionalised with foundation diameter (D), and the water depth (h) also non-dimensionalised by foundation diameter.

Figure 4 presents scour data for built or under construction Round 1 and 2 wind farm sites as well as the Princess Amalia OWF in the Dutch Sector. The deepest scour recorded at Round 1 developments was at the Scroby Sands site (S/D = 1.38). In data from the Round 2 Robin Rigg site the foundation-averaged scour depth is up to S/D = 1.77, with the majority of locations being less, in a similar range of water depths. The main clusters of data for Scroby Sands and Robin Rigg are deeper than the single value that was available for Arklow Bank. However, there is scatter in the S/D values for Robin Rigg such that the observations cover the range of existing predictive equations, i.e. 1.3D to 1.75D, and some foundations have lower periods of time between installation and survey which limits the scour development at the time the survey was taken. The data from Princess Amalia is in a cluster, with scour depths generally up to S/D = 0.81, with one value deeper at S/D = 1.15. The most recent data for Kentish Flats in a clay environment has values of S/D up to 0.4. There is some evidence for fluctuations in scour with time at Kentish Flats, with two foundations apparently experiencing progressive scour depth increase with time. The data for Barrow shows low (no) scour in the clay sites. The newest data from North Hoyle (not plotted) shows evidence of little (no) scour around the foundations, which is in line with the results presented in Whitehouse *et al.* (2008).

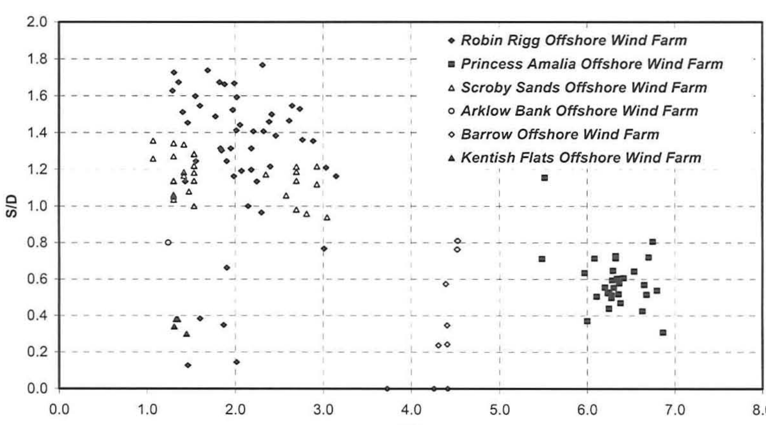

Figure 4. Non-dimensional plot of scour depth (S) data for offshore wind farms with no foundation scour protection in place (Note: D is monopile diameter and h is water depth to mean sea level). (COWRIE, 2010).

The maximum S/D values are broadly in agreement with the range suggested by Breusers and Raudkivi (1991). They suggested a value of $S/D = 2.3$ when the flow velocity was four times the sediment threshold velocity. Below this condition they adopted a graphical approach to determining the multiplier based on experimental evidence. This is also in line with the approach given in Sumer and Fredsøe (2002) where the mean value of $S/D = 1.3$ allows for a standard deviation term of 0.7 to be added, which would give an upper value of $S/D = 2.0$.

As has been noted previously in DECC (2008) the data analysed supports the view that scour is a progressive process where the seabed sediment is naturally mobile, and there is an adequate thickness of that sediment for scouring to occur. Where the seabed is comprised of stiff clay, there is a superficial layer of sediment overlying clay or the wave and current conditions are not generally strong enough to cause the seabed sediment to be naturally mobile, the scour will be slower or limited.

ENVIRONMENTAL DATA REQUIREMENTS

In shallow water wave orbital velocities at the seabed are the critical wave parameter for estimating scour hazard. These are usually estimated from wave height and period using wave theory rather then being measured directly. A rigorous assessment of scour hazard would require some quantification of day to day wave activity in addition to extreme values. It would also be necessary to quantify how wave parameters vary with time and how long they persist above given thresholds, perhaps by characterising the typical frequency and duration of storms. A probabilistic approach might be appropriate where for example the cumulative frequency distributions of significant wave height are fitted to a well-known distribution such as the three-parameter Weibull distribution. In some locations it would also be necessary to quantify tidal and longer period variations in water level where these are large enough to affect the wave conditions.

In relatively deep water the influence of waves can (often) be neglected and scour hazard is likely to be controlled by currents. The depth at which wave action can be neglected will depend upon the wave climate at the site in question, so wave particle velocities at the seabed should be estimated for extreme wave conditions to determine potential scour hazard. In the simplest case, currents can be represented by an extreme value of current speed at 1 m above the seabed. These values are commonly derived using well-established techniques and an appropriate return period value should be selected according to the engineering application.

It is very important to know the surficial soil characteristics for a scour assessment, data starting from 1 m below the bed in a site investigation may not be representative of the surface sediment properties, but will be important for scour greater than 1 m deep. The influence of layering in the sandy and silty soils or the presence of a veneer of mobile sediment overlying, for example, stiff clay need to be taken into account in the assessment. Construction effects on soil properties must also be considered if these are expected to change the soil properties related to the foundation.

FUTURE RESEARCH

As well as maintaining the existing evidence base as new data becomes available, there are four distinct but related areas in which further research will lead to benefits in understanding and predicting scour response. The first relates to the time variation in scour at sandy sites; the second to scour potential and scour development with time in heteregeneous soils (gravel-sand-silt-clay mixtures); the third relates to complex foundation structures (gravity base, jacket and multi-leg foundations), and the fourth relates to the optimisation of scour protection performance for monopile and complex foundation structures:

(1) There is an issue of time development of scour holes in a varying wave and current environment and this can have implications for foundations, cabling and the placement of scour protection. Detailed time-series measurements of scour and environmental conditions are required to validate (or improve) existing models.

(2) There is uncertainty of scouring around foundations in heterogeneous soils and, currently, there is no specific guidance as to how best to assess scour potential in such situations. The Earth Materials approach (Annandale, 2006) shows promise and there is a requirement for a review of available methods in light of actual environmental conditions experienced, site data on soils, and observed scour development offshore. Once this review has been completed recommendations can be made for the most appropriate approaches to adopt.

(3) There is little evidence as to the performance of installed scour protection around existing OWF sites (e.g. other than DECC, 2008). The scour protection that has been placed appears to be effective in preventing bed lowering adjacent to the foundations, although filter layers appear to be necessary to prevent settlement of rock armour layers. Where material has been placed in the scour hole, and the top level is above the level of the surrounding seabed level, it is evident that the mound of protection material has produced a secondary scour response in mobile sediment environments. Further analysis of measurements of scour protection level and profile would be useful, combined with visual information to show how the surface of the scour protection material varies with time (e.g. armouring, infill with fines).

This will inform the production of guidance on the role of placement methodology in the evolution of the scour protection and the interaction of the protection with the surrounding seabed. In the longer term data will be required to evaluate the scour protection performance under the influence of regional changes in bed level (e.g. on sandbanks, sandwaves and due to channel movement).

(4) For foundation structures other than monopiles it is necessary to use a combination of approaches to estimate likely scour around the foundation. The general suitability of these approaches acts as an uncertainty in the design process. Further, the representation of more complex foundation types in the typical shallow water coastal modelling systems that are used in the environment assessments is a large uncertainty. This uncertainty can be reduced through a programme of detailed laboratory experiments combined with numerical modelling. This approach is of particular interest when determining how to deal with other non-standard foundation shapes, such as those encountered with seabed mounted wave energy devices.

ACKNOWLEDGEMENTS
The research was made possible through the support of offshore wind farm developers in providing data to inform the COWRIE and DECC work. With respect to results included from the COWRIE work specific acknowledgement is made to E.ON, Climate & Renewables UK for allowing the use of scour monitoring data from the Robin Rigg Offshore Wind Farm, and Van Oord Dredging and Marine Contractors BV for allowing the use of scour monitoring data from the Princess Amalia Wind Farm. The views, results and conclusions are those of the authors and not necessarily those of the funders or those providing the data. Support for additional research and preparation of the paper came from the company research programme of HR Wallingford.

REFERENCES

Annandale, G.W. (2006). *Scour Technology.* Mechanics and Engineering Practice. McGraw-Hill.

Breusers, H.N.C. and Raudkivi, A.J. (1991). *Scouring.* IAHR Hydraulic Structures Design Manual, 2, A. A. Balkema, Rotterdam, vii + 143 p.

Byrne, B. W. and Houlsby, G.T. (2003). Foundations for offshore wind turbines. *Phil. Trans. R. Soc. Lond. A*, 361, 2909-2930.

COWRIE (2010). *A Further Review of Sediment Monitoring Data.* Final Report prepared by ABPmer Ltd, HR Wallingford Ltd and CEFAS for the Research Advisory Group, Project Ref. ScourSed-09, March, 115 p.

DECC (2008). *Dynamics of scour pits and scour protection – Synthesis report and recommendations (Milestones 2 and 3).* Final Report prepared by HR Wallingford Ltd, ABPmer Ltd and CEFAS for the Research Advisory Group, Department of Energy and Climate Change (DECC) and Department for Environment, Food and Rural Affairs (Defra).

Harris, J.M., Whitehouse, R.J.S. and Benson, T. (2010). The time evolution of scour around offshore structures. *Proceedings of the Institution of Civil Engineers, Maritime Engineering*, 163, March, Issue MA1, 3 – 17.

Sumer, B.M. and Fredsøe, J. (2002). *The Mechanics of Scour in the Marine Environment.* Advanced Series on Ocean Engng., Vol. 17, World Scientific, Singapore. xiii + 536 p.

Whitehouse, R.J.S (1998). *Scour at marine structures: A manual for practical applications.* Thomas Telford, London, 198 p.

Whitehouse, R. (2006). Scour at coastal structures (Invited lecture). *Proceedings Third International Conference on Scour and Erosion, November 1-3, pp. 52-59, © CURNET, Gouda, The Netherlands [CD-ROM].*

Whitehouse, R., Harris, J., Sutherland, J. and Rees, J. (2008). An assessment of field data for scour at offshore wind turbine foundations. *Proceedings Fourth International Conference on Scour and Erosion, Tokyo, Japan, Paper B-13, 329-335.*

Physics of Rock Scour: the Power of the Bubble

E.F.R. Bollaert[1], M. ASCE

[1] President, AquaVision Engineering, Chemin des Champs-Courbes 1, CH-1024 Ecublens, Switzerland, PH +41(0)797751761, email: erik.bollaert@aquavision-eng.ch

ABSTRACT

Scour of rock downstream of high-head hydraulic structures is governed by multiphase physics of turbulent air-water mixtures impacting and eroding fractured rock. The present paper provides first of all an overview of the main physical processes and focuses on relevant break-up mechanisms of rock. Particular emphasis is given to the influence of air bubbles present in the water on scour formation. Also, relevant scaling issues are pointed out for each of the processes.

Second, based on these processes, a physics-based near-prototype scaled engineering model for scour predictions, the Comprehensive Scour Model (CSM), is being presented, as well as feedback on applications of the model to case studies and real-life projects. The CSM has been initiated in 2001 and since then been further developed and completed by applying it to real-life rock scour problems at high-head dams worldwide.

All in all, it appears that the gas phase significantly influences all stages of scour development, from the issuance of the flow at the dam crest to the formation of the scour hole downstream. The power of the air bubble reveals to be beyond our expectations.

PHYSICS OF ROCK SCOUR

Fluvial erosion of rock as it appears in the vicinity of engineering structures generally occurs following a sequence of physical-mechanical processes as illustrated at Figure 1. This figure distinguishes between the fall of an aerated water jet, the impact and diffusion of the jet through the plunge pool, the generation of dynamic pressure fluctuations at the water-rock interface, and finally instantaneous (dynamic block ejection, sudden joint break-up) and time-dependent (abrasion, progressive joint break-up, downstream displacement) rock break-up processes. Three rock break-up processes are being described more in detail:

1. rock block removal (by pressure differences in joints or shear flow),
2. rock mass fracturing (suddenly or progressively),
3. rock block peeling off (combination of removal/fracturing).

Each of these processes has its own time-scale of occurrence, ranging from instantaneous to long term. While sudden break-up actions such as block uplift are described in literature, sound assessment of progressive break-up by fracturing and peeling off of blocks are still in their initial phases of development. Their relevance to scour depends on the characteristics of the turbulent flow and on the shape and the protrusion of the rock blocks. For small-sized rocky material, shear flow is generally predominant, just like for a granular riverbed. For large-sized irregular rock blocks, however, the shape, dimensions and protrusion of the blocks significantly impact the failure process.

In the following, the physics of how a rock fails are explained more in detail as well as the corresponding computational modules being part of the CSM. Emphasis is thereby given to the influence of the air bubble presence in the water.

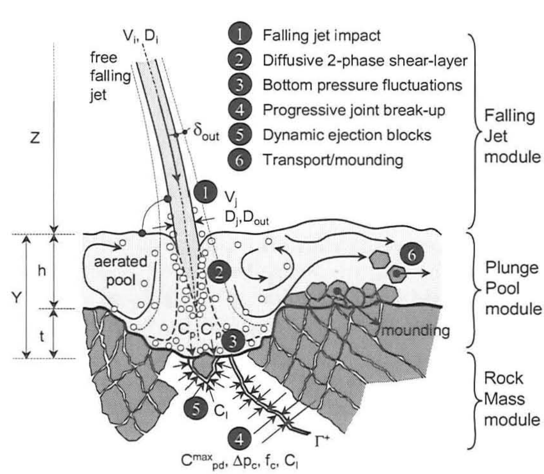

Figure 1. Physical-mechanical phenomena responsible for break-up of rock.

Rock block removal

Rock may fail by removal of distinct blocks. This may happen by uplift (quasi-vertical ejection), by horizontal displacement (shear), or by a combination of both. Beside average flow velocities and pressures near the bottom, flow turbulence is generally of importance. Which of the movements and forces are most plausible depends on the size, dimensions and protrusion of the blocks compared to the surrounding rock mass. These parameters directly define the relevance of the quasi-steady and turbulent forces that may lift the block. For non-protruding blocks, only turbulent forces enhance block uplift. For highly protruding blocks, flow deviating quasi-steady forces are predominant. The Dynamic Uplift (DI) module of the CSM allows computation of uplift heights of distinct rock blocks.

Rock mass fracturing

Rock may also fail by sudden or progressive hydraulic fracturing, which is mathematically described by the theory of linear elastic fracture mechanics. Brittle fracture occurs when the stress intensity at the edges of closed-end fractures is greater than the in-situ fracture toughness of the rock (Bollaert, 2002). The stresses induced by water pressures are governed by the geometry of the fracture and the support of the surrounding rock. The in-situ fracture toughness of the rock depends on the type of rock, its unconfined compressive strength (UCS) and the in-situ stress field.

Second, progressive fracturing of rock occurs when the stress intensities do not exceed the fracture toughness. Prototype-scaled laboratory tests have shown the presence of air-water transient waves inside rock joints (Bollaert, 2002; Bollaert & Schleiss, 2005). These generate cyclic pressures that, on the medium or long term, may propagate an existing fracture by fatigue, depending on the number and the intensity of pressure pulses. This failure type is time-dependent and takes an end when fracture formation is completed. The Comprehensive Fracture Mechanics (CFM) module of the CSM computes both brittle and fatigue fracturing as a function of duration of flooding.

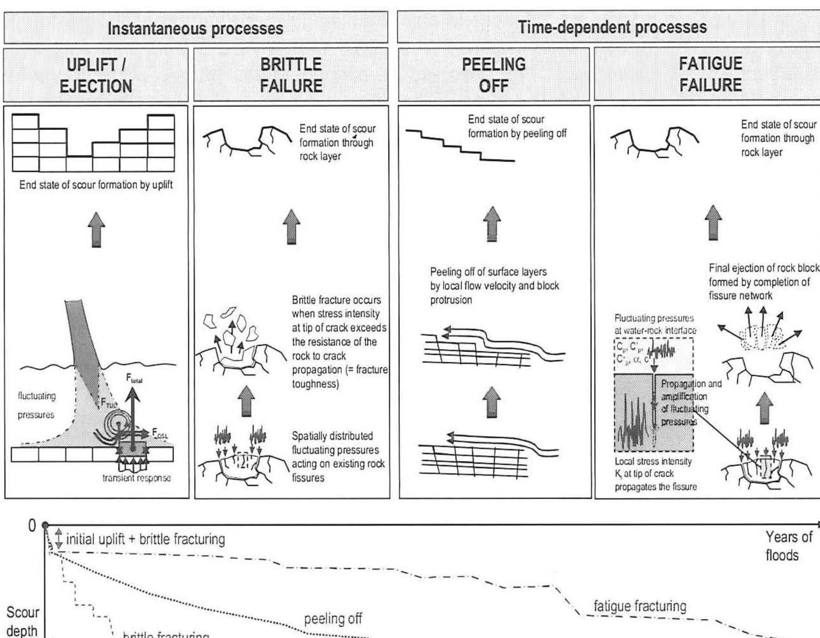

Figure 2. Principle failure mechanisms of fractured rock at hydraulic structures

Rock block peeling off

Peeling off of blocks is a specific combination of both quasi-steady pressure forces and brittle or fatigue fracturing. The phenomenon typically occurs in layered rock. The destabilizing forces are not only due to flow turbulence, but are also generated by a strong local flow deviation due to protrusion of the block. This flow deviation generates drag and lift forces on the exposed faces of the block, which are governed by the relative importance of the protrusion of the block and by the local quasi-steady flow velocity in its immediate proximity.

The corresponding pressures may develop brittle or fatigue fracturing of the joint between the block and the underlying rock. In case the exposed block is detached or almost detached, no further fracturing is needed to uplift the block by pressure fluctuations entering laterally into the joint. The Quasi-Steady Impulsion (QSI) module of the CSM computes peeling off of distinct rock block layers, which is particularly relevant in the case of regressive scour towards the toe of the dam of appurtenant structure.

THE POWER OF THE BUBBLE

For each of the described processes, several phases and forces work together. As such, scaling effects are inherent to any small-scale reproduction of the prototype behavior of the process in question. For aerated falling jets, Weber and Reynolds numbers are of importance. For processes occurring in the plunge pool, Reynolds numbers are often very small and air entrainment and air transfer to the bottom are both incorrect. Inside rock joints, different geometrical scales as well as different air-water wave celerities are source of discrepancies. As such, air bubbles are at the base of most of the scaling issues in rock scour because unfortunately present in all of the aforementioned physical processes. This is illustrated in Figure 3.

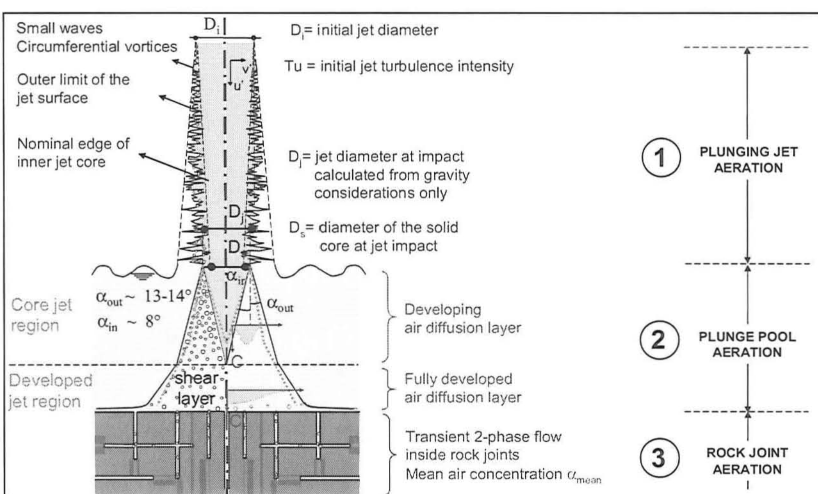

Figure 3. Air entrainment of jet, pool and rock mass.

Jet issuance from the dam

Jet issuance conditions reproduced on a laboratory (small) scale are often affected by the following scaling effects:

1. initial jet turbulence intensity and thus air entrainment is too low
2. jet deflection angle (lip) is different than the prototype deflection angle
3. approach flow conditions in the upstream reservoir are not representative

Relevant initial jet turbulence intensities for prototype jets are between 3 and 8 % (Ervine & Falvey, 1987). The turbulence intensity is directly responsible for jet aeration and jet spread during its fall. A more detailed discussion of jet turbulence as a function of type of issuance conditions can be found in Manso et al. (2006).

Jet fall through the air

During its fall, a scaled jet exhibits the following effects:

1. inner and outer spread angles are too low
2. jet air entrainment is too low
3. shape of the jet does not deform as on prototype
4. jet trajectory does not account for air drag and wind effects

Air drag during fall is generally accounted for by means of a trajectory reduction. Air entrainment is impossible to correctly reproduce on a scale model. Shape deformation of jets during fall is very difficult to correctly reproduce at small scales.

Jet diffusion through the water cushion

When diffusing through the water cushion of the downstream plunge pool or stilling basin, the following scaling effects occur:

1. plunge pool quantity (mass) of air and volume of air at impact are low because jet velocity at impact is low
2. plunge pool water level is too stable and does not fully account for local recirculation patterns and instabilities that might be present on the prototype
3. plunge pool quantity of air (mass) at the bottom is too low
4. plunge pool volume of air at the bottom is generally too high because of the wrong quantity of air in the pool and of the lack of stagnation pressures.

Aeration aspects in pools are very complex and have been extensively studied at prototype scale by Bollaert et al. (2009). Due to stagnation, prototype water cushions exhibit a strong pressure gradient near the bottom, reducing the air volume based on the ideal gas law, whereas scaled cushions are not able to reproduce this gradient. As such, despite the low aeration at impact (due to scaled jet velocities), air volume at the bottom is generally overestimated on scale models. As such, the corresponding mean dynamic pressures are underestimated near the bottom.

Air concentrations (void fractions) were measured by means of a double fibre-optical probe on a near-prototype scaled facility. Three measurement points (MP) were selected inside the pool (Figure 4): 1) in the impingement zone of the jet (MP1), 2) in the transition to the wall jet region (MP2) and 3) just above the impinging jet region (MP3), 10 cm above the pool floor for different pool depths.

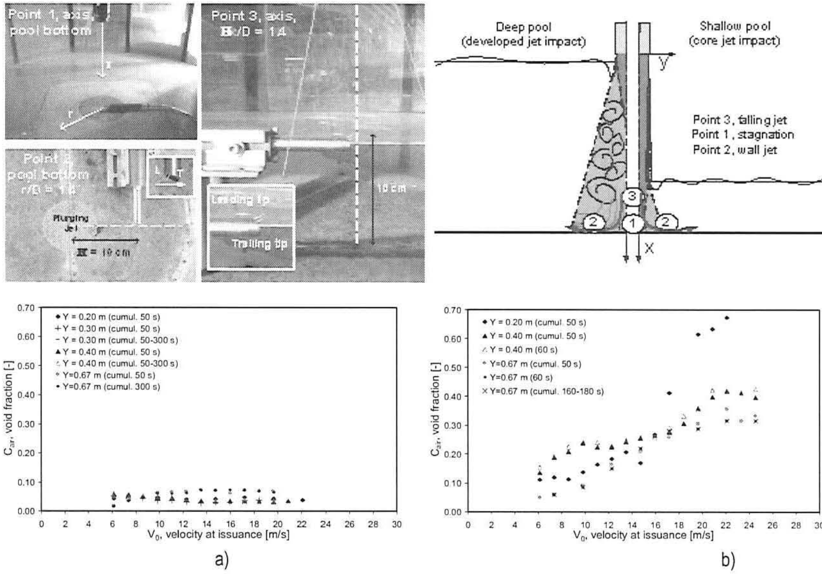

Figure 4. Upper part: Positioning of optical probe and measurement points of void fraction. Lower part: Void fractions measured for different pool depths: a) at point 1 (MP1) located at the jet stagnation point (centre); b) at point 2 (MP2), in the wall jet region away from the stagnation point.

The results are presented as a function of jet issuance velocity for Y/D between 2.8 and 9.3, in which Y stands for the plunge pool depth and D for the jet diameter at impact. At the jet's stagnation point, measured void fractions were between 2 and 8 %, regardless of the jet velocity. Radially away from the stagnation point, but still along the pool floor, void fractions highly depended on the jets' issuance velocity and reached up to 40 %.

In other terms, at low jet velocities (V < 10 m/s), void fractions at the jet's stagnation point are quite similar to the ones measured radially outwards, while at high jet velocities, (V > 20 m/s), void fractions at the jet's stagnation point are 5-6 times less than the ones measured radially outwards. A similar trend has been observed at measurement point 3.

Void fractions are directly related to the pressure built-up when approaching the jet's stagnation point and to the sudden pressure decrease following radial jet deflection after pool floor impact. By applying the ideal gas law, the volume reduction ΔV of a given quantity (mass) of air is inversely proportional to the rise in absolute pressure Δp. The amount of air does not change, only the size of the bubbles changes due to a variation of absolute water pressure.

The air content at the water-rock interface influences the pressures inside the rock joints. Once the air bubbles transferred inside the joint, pressure fluctuations increase or decrease the corresponding volume of the mass of bubbles in a cyclic manner. Also, the mass of free air may change according to Henry's law. The presence of air inside the joint significantly modifies the compressibility of the air-water mixture and thus its ability to generate oscillations and resonance waves inside the joints (see further). As such, air bubbles are at the base of the hydraulic jacking power of a high-velocity jet. More details can be found in Bollaert (2002, 2004).

Bottom pressure fluctuations

Due to the significantly different turbulence and air entrainment characteristics of a small-scale pool or stilling basin, the related turbulent pressure fluctuations at the interface are also not fully representative (Bollaert et al., 2002):

1. maximum and minimum extreme pressures are too low
2. RMS (root-mean-square) values are too low
3. very high and very low frequencies are not present at small scales
4. spatial distribution of pressure fluctuations is too centralized

Hence, prototype pressures at the pool bottom are different from pressures measured on scale model facilities. Both the root-mean-square values and the extreme values are significantly higher on prototype, and the corresponding frequency spectra have considerable energy even at high frequencies. Moreover, the zone at the pool bottom that is influenced by the turbulent shear layer of the impacting jet is not well defined in reality and can extend over a wide area due to aeration and lateral displacements of the point of impact of the jet in the pool.

Rock joint pressure fluctuations

Pressures travel through joints as two-phase transient waves, whereby the jet acts as an exciter and the joint as a resonance chamber. Oscillations and extreme values are strongly depending on the air content inside the joint, as well as on the geometry (length, shape) of the joint. Small scale models are unable to correctly account for these effects. Air influence on net uplift pressures is shown in Figure 7.

Near-prototype scaled laboratory tests have shown that pressure pulses inside artificially generated rock joints may exhibit amplifications of several times the corresponding pressure pulse at the water-rock interface (entrance of the joint). This clearly points out the importance of the air presence and is illustrated at Figure 5.

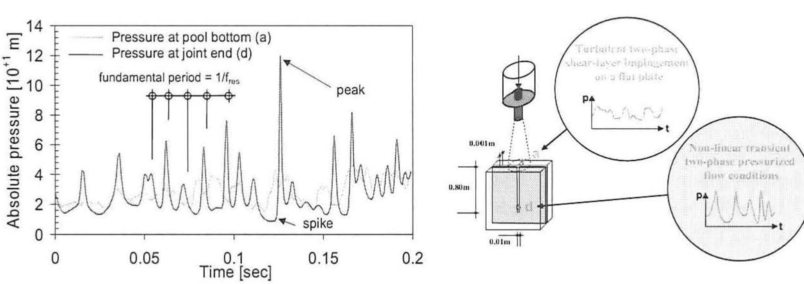

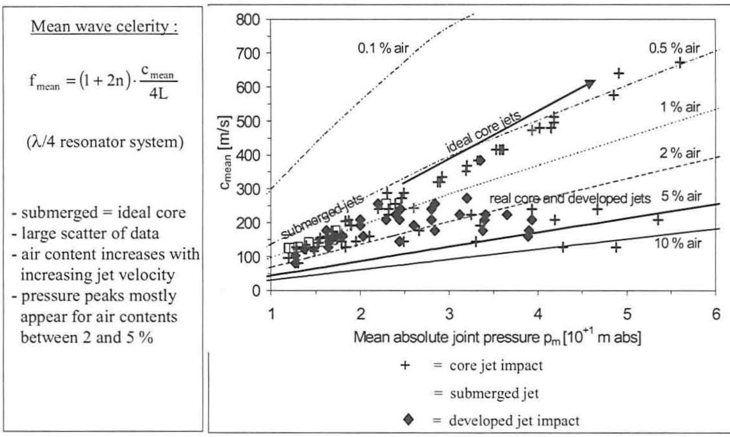

Figure 5. Air concentrations and mean wave celerities inside rock joints impacted by aerated and non-aerated (submerged) high-velocity jets.

Rock mass resistance to scour

Small-scale physical models often make use of binders such as cement, clay, etc. to simulate the resistance of partially fractured rock against scour. This, however, has proven to be unreliable and unable to accurately model both the real shape and the extent of a plunge pool scour hole.

It is evident that mixtures of sand/gravel and binders cannot replace the much more complex prototype behavior of rock when it comes to fracturing processes and dynamic ejection of rock blocks. The former process is governed by the fracture toughness of the rock mass and by the real geometry of the joints. The latter process depends on dynamic pressure pulses over and under the blocks, which are directly related to local turbulent conditions near the block in question.

Typical shortcomings of scale models are the lack of steep slopes of the modeled scour hole, and the appearance of a downstream mound that is way too important. Unfortunately, both aspects have significant influence on scour formation.

THE COMPREHENSIVE SCOUR MODEL (CSM)

A physics based scour prediction model, the Comprehensive Scour Model (Bollaert, 2002, 2004; Bollaert & Schleiss, 2005), has been developed based on the aforementioned processes. It is called comprehensive in the sense that it incorporates the major physics relevant to scour in an easily understandable manner, i.e. by using mathematics of the physical laws that are both representative for the phenomena in question but at the same time easy to understand.

The model is applicable to any kind of brittle fractured medium, i.e. fractured rock, strong clays, concrete, etc. Typical fields of application are spillways and stilling basins, bridge piers, concrete fracturing of spillway chutes, uplift of stilling basin concrete linings, uplift of anchored sidewalls and protection slabs, a.s.o.

It uses linear elastic fracture mechanics to express hydraulic jacking in the fractured medium of interest. Second, dynamic uplift of blocks of the fractured medium due to net uplift forces and impulsions is being simulated. The hydraulic action for each failure mechanism is determined along the scour critical parts of the liquid-solid interface. The scour resistance of the fractured medium is expressed by its main geomechanical characteristics. Interaction between the progressing scour hole and its influence on the hydraulic action is being accounted for.

The model computes failure of fractured rock by fracturing, uplift or peeling off. The structure consists of 3 modules: the falling jet, the plunge pool and the rock mass. The latter directly implements the different failure mechanisms.

Falling Jet Module

This module describes how the hydraulic and geometric characteristics of the jet are transformed from dam issuance down to the plunge pool (Figure 1). Three main parameters characterize the jet at issuance: the velocity V_i, the diameter (or width) D_i and the initial turbulence intensity Tu, defined as the ratio of velocity fluctuations to the mean velocity. The jet trajectory is based on ballistics and air drag. The jet module computes the longitudinal location of impact, the total trajectory length L and the velocity and diameter at impact V_j and D_j.

Plunge Pool Module

This module describes the characteristics of the jet when traversing the plunge pool and defines the water pressures at the water-rock interface. The plunge pool water depth Y and bottom shape are essential. The water depth Y and jet diameter at impact D_j determine the ratio Y/D_j, which is directly related to jet diffusion. The most relevant pressures are the mean dynamic pressure coefficient C_{pa} and the root-mean-square (rms) coefficient of the fluctuating dynamic pressures C'_{pa}, both measured directly under the centerline of the jet. These coefficients are influenced by the degree of confinement of the pool bottom, generating upward oriented return currents that enhance energy dissipation inside the pool.

Rock Mass Module

The pressures at the bottom are used for determination of pressures inside rock joints. The main parameters are: the maximum dynamic pressure coefficient C^{max}_{p}, the characteristic amplitude Δp_c and frequency f_c of pressure cycles and the maximum dynamic impulsion coefficient C^{max}_{I}. The first parameter is relevant to brittle propagation of closed-end rock joints. The second and third parameters express time-dependent propagation of closed-end rock joints. The fourth parameter is used to define dynamic uplift of rock blocks formed by open-end rock joints.

The maximum dynamic pressure C^{max}_p is obtained through multiplication of the rms pressure C'_{pa} with an amplification factor Γ^+, and by superposition with the mean dynamic pressure C_{pa}. The amplification depends on the air content and the product of C'_{pa} times Γ^+ results in a maximum pressure, written as (Bollaert, 2002 & 2004):

$$P_{max}[Pa] = \gamma \cdot C_p^{max} \cdot \frac{V_j^2}{2g} = \gamma \cdot \left(C_{pa} + \Gamma^+ \cdot C'_{pa}\right) \cdot \frac{V_j^2}{2g}$$

The characteristic amplitude of the pressure cycles, Δp_c, is determined by the maximum and minimum pressures of the cycles. The characteristic frequency of pressure cycles f_c follows the assumption of a perfect resonator system (see Figure 5) and depends on the air concentration in the joint α_i and on the length of the joint L_f.

Comprehensive Fracture Mechanics (CFM)

The resistance of the rock against fracture propagation has to be determined. The cyclic character of pressures in joints makes it possible to describe joint propagation by fatigue stresses occurring at their tip. This can be described by Linear Elastic Fracture Mechanics. Joint propagation distinguishes between brittle and time-dependent propagation. The former happens for a stress intensity equal to or higher than the fracture toughness of the rock. The latter is occurring in the opposite case. Joints may then be propagated by fatigue. Failure by fatigue depends on the frequency and the amplitude of the load cycles. Stresses are characterized as follows:

$$K_I = P_{max} \cdot F \cdot \sqrt{\pi \cdot L_f}$$

in which K_I is in MPa$\sqrt{m}$ and P_{max} in MPa. The boundary correction factor F depends on the type of crack and on its persistency, defined as a/B or b/W in Figure 6.

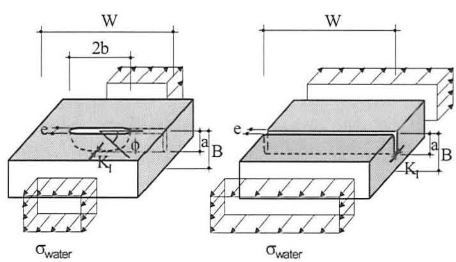

Figure 6. Types of rock joint configurations modelled in the CSM.

This figure presents two basic configurations for partially jointed rock. The choice of the most relevant geometry depends on the type and the degree of jointing of the rock. The first crack is of semi-elliptical shape and partially sustained by the surrounding rock mass in two horizontal directions. Corresponding stress intensity factors should be used in case of low to moderately jointed rock. The second crack is single-edge notched and of two-dimensional nature. Support from the surrounding rock mass is only exerted perpendicular to the plane of the notch and, as a result, stress intensity factors will be substantially higher. Thus, it is appropriate for significantly to highly jointed rock. For practice, F values of 0.5 or higher are considered to correspond to completely broken-up rock, i.e. dynamic uplift becomes more relevant than fracturing. For values of 0.1 or less, a tensile strength approach is more plausible.

However, most of the values in practice can be considered between 0.20 and 0.40, depending on the type and number of joint sets, the degree of weathering, joint interdistances, etc. The fracture toughness K_{Ic} has been related to the mineralogical type of rock and to the unconfined compressive strength UCS. Furthermore, corrections are made to account for the loading rate and the in-situ stress field. Hence, the in-situ fracture toughness $K_{I,ins}$ is based on literature data and written as:

$$K_{I\ ins,\ UCS} = (0.008\text{-}0.010)\cdot UCS + (0.054\cdot\sigma_c) + 0.42$$

in which σ_c represents the confinement horizontal in-situ stress and T, UCS and σ_c are in MPa. Instantaneous joint propagation will occur if $K_I \geq K_{I,ins}$. If this is not the case, joint propagation is expressed as follows:

$$\frac{dL_f}{dN} = C_r \cdot \left(\Delta K_I / K_{Ic}\right)^{m_r}$$

in which N is the number of pressure cycles. C_r and m_r are material parameters that are determined by fatigue tests and ΔK_I is the difference of maximum and minimum stress intensity factors. To implement time-dependent joint propagation into the model, m_r and C_r have to be known. A calibration for granite (Cahora-Bassa Dam; Bollaert, 2002) resulted in C_r = 1E-8 for m_r = 10.

Dynamic Impulsion (DI)

The last hydrodynamic parameter of importance is the maximum dynamic impulsion C^{max}_I in an open-end joint (underneath single block), obtained by time integration of net forces on the block (pressures under and over block, immerged weight of block and eventually shear and interlocking forces).

$$I = \int_0^{\Delta tpulse} \left(F_u - F_o - G_b - F_{sh}\right) \cdot dt = m \cdot V_{\Delta tpulse}$$

in which F_u and F_o are the forces under and over the block, G_b is the submerged weight of the block and F_{sh} represents the shear and interlocking forces. The shape of a block and the type of rock define the immerged weight. Shear and interlocking forces depend on the joint pattern and the in-situ stresses. As a first approach, they can be neglected. The pressure field over the block is governed by jet diffusion. The pressure field under the block corresponds to transient pressure waves.

Uplift of a block may be computed by defining at each time instant the uplift forces on the block, together with the resistant forces defined by its mass and by eventual shear and interlocking forces between the block and the surrounding rock. The force balance has to be established following the potential orientation of movement.

The first step is to define the maximum net impulsion I_{max}. I_{max} is defined as the product of a net force and a time period. The corresponding pressure is made non-dimensional by the jet's kinetic energy $V^2/2g$. This results in a net uplift pressure coefficient C_{up}. The influence of air presence on this coefficient is shown in Figure 7 (left side). The time period is made non-dimensional by the travel period that is characteristic for pressure waves inside rock joints, i.e. $T = 2\cdot L_f/c$. This results in a time coefficient T_{up}. Hence, the non-dimensional impulsion coefficient CI is defined by the product $C_{up} \cdot T_{up} = V^2 \cdot L/g \cdot c$ [m·s]. The maximum net impulsion I_{max} is obtained by multiplication of C_I by $V^2 \cdot L/g \cdot c$. Prototype-scaled analysis of uplift pressures resulted in the following expression for C_I:

$$C_I = 0.0035 \cdot \left(\frac{Y}{D_j}\right)^2 - 0.119 \cdot \left(\frac{Y}{D_j}\right) + 1.22$$

Failure of a block is expressed by the displacement it undergoes due to the net impulsion coefficient C_I. This is obtained by transformation of $V_{\Delta tpulse}$ into a net uplift displacement h_{up}. The net uplift displacement that is necessary to eject a rock block from its matrix is difficult to define. It depends on the protrusion and the degree of interlocking of the blocks. A calibration on Cahora-Bassa Dam (Bollaert, 2002) resulted in a critical net uplift displacement of 0.20.

Nevertheless, in reality, block movement and uplift forces are highly correlated. Experimental research is actually ongoing at the Swiss Federal Institute of Technology in Lausanne to solve this complex correlation (Federspiel et al., 2009). An artificial rock block has been equipped with pressure and acceleration sensors to detect the direct relation between the pressures over and under the block and its detailed movements. The block is being impacted by a near-prototype air-water jet.

Quasi-Steady Impulsion (QSI)

Peeling off of rock blocks is a specific combination of both quasi-steady forces and brittle or fatigue fracturing. The phenomenon typically occurs in layered rock, such as sedimentary rock. If is often responsible for regressive erosion towards the toe of the dam. The destabilizing forces are not due to flow turbulence alone, but are principally generated by the flow deviation due to a protrusion "e" of the block along the bottom (e_{block} in Figure 7, right side). This flow deviation generates drag and lift forces on the exposed faces of the block, which are governed by the relative importance of the protrusion of the block into the flow and by the local quasi-steady flow velocity in the immediate proximity of the block ($V_{backflow}$ in Figure 7).

These forces may develop brittle or fatigue fracturing of the joint between the block and the underlying rock mass. In many cases, the exposed block is detached or almost detached and no further fracturing is needed to uplift the block from its mass.

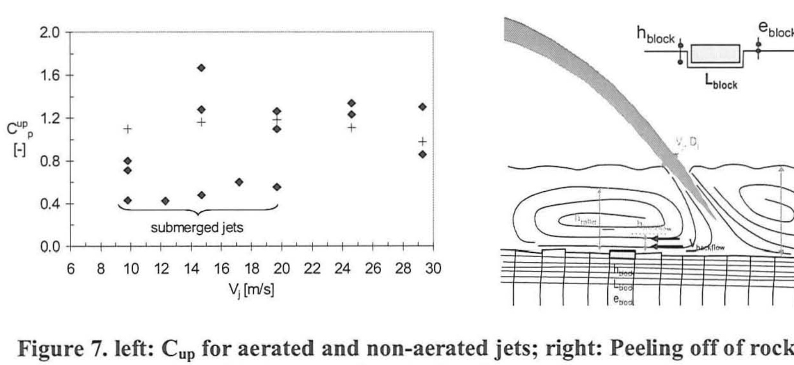

Figure 7. left: C_{up} for aerated and non-aerated jets; right: Peeling off of rock blocks at surface during flow event.

APPLICATION TO KARIBA DAM (ZAMBIA-ZIMBABWE)

Kariba Dam is a 128 m high concrete arch dam on the Zambezi River, situated on the border between Zambia and Zimbabwe. Since 1962, spillway discharges from Kariba Dam have eroded an important scour hole into the gneiss rock, which extends since 1982 about 80 m below the initial river bed (Mason & Arumugam, 1985).

Use of estimated annual flood periods and in-situ measured scour formation allowed calibrating the CSM model to predict future scour formation as a function of time (Bollaert, 2005). Especially the time-related parameters of the CSM model have been adapted to the long-duration observed prototype scour (20 years of scour follow-up between 1962 and 1981).

After dam construction in 1959, a large scour hole quickly formed in the downstream fractured rock. Typical spillway discharges and average tailwater levels are available, and the average time duration of floods has been estimated at about 3 months. Furthermore, after each major flood period between 1962 and 1981, a detailed bathymetric survey of the scour hole has been carried out. Results of these surveys can be found in Mason & Arumugam (1985).

The spillway consists of 6 rectangular gate openings of roughly 8.8 m by 9.1 m, for a total discharge of about 9'500 m^3/s. The gate lips are situated at 456.5 m a.s.l. The minimum and maximum reservoir operating levels are 475.5 and 487.5 m a.s.l. The downstream tailwater level is situated between 390 and 410 m a.s.l., depending on the number of gates functioning. An average value of 400 m a.s.l. has been assumed for the computations. The net head difference results in typical jet outlet velocities of 21.5 m/s.

Scour formation in the rock mass reached a level of 306 m a.s.l. in 1981, i.e. about 80 m down the initial bedrock level. The rock mass is sound gneiss with a degree of fracturing that is not known precisely. Without further noticeable information on the rock mass quality, the computations have been performed for a set of conservative, average and beneficial parametric assumptions. Parametric analysis points out the influence of this uncertainty on the computed scour formation.

The spillway discharges are generally performed for varying gate numbers, gate openings and operations, as a function of already formed scour. This results in complex and varying hydraulics. In the following, a 2D simplified approach is considered, assuming only one jet and a (considered reasonable) average gate opening of 75 %. The time durations of the floods also vary from year to year. Nevertheless, it is considered that the flood season generally takes several months in this region. Hence, an average duration of 3 months or 90 days per year has been assumed for the scour computations.

Table 1 summarizes the parametric assumptions made for the rock properties. The main scour influencing parameters are the UCS (Unconfined Compressive Strength) strength, the initial degree of fracturing and the form of the joints.

Scour evolution with time is presented in Figure 8 for a range of different UCS strengths. Significant differences in scour formation are observed, underlying the need for sound UCS knowledge. Especially at lower UCS strengths, scour formation becomes sensitive to the absolute value. Based on the in-situ measured scour hole, the rock mass strength to be used in the calibrated CSM should be between 75 and 100 MPa.

Table 1. Rock mass properties under different parametric assumptions

Property	Symbol	CONSERV	AVERAGE	BENEF	Unity
Unconfined Compressive Strength	UCS	100	125	150	MPa
Density rock	γ_r	2600	2700	2800	kg/m^3
Typical maximum joint length	L	1	1	1	m
Vertical persistence of joint	P	0.12	0.25	0.55	-
Form of rock joint	-	single-edge	elliptical	circular	-
Tightness of joints	-	tight	tight	tight	-
Total number of joint sets	N_j	3+	3	2+	-
Typical rock block length	l_b	1	1	1	m
Typical rock block width	b_b	1	1	1	m
Typical rock block height	z_b	0.5	0.75	1	m
Joint wave celerity	c	150	125	100	m/s

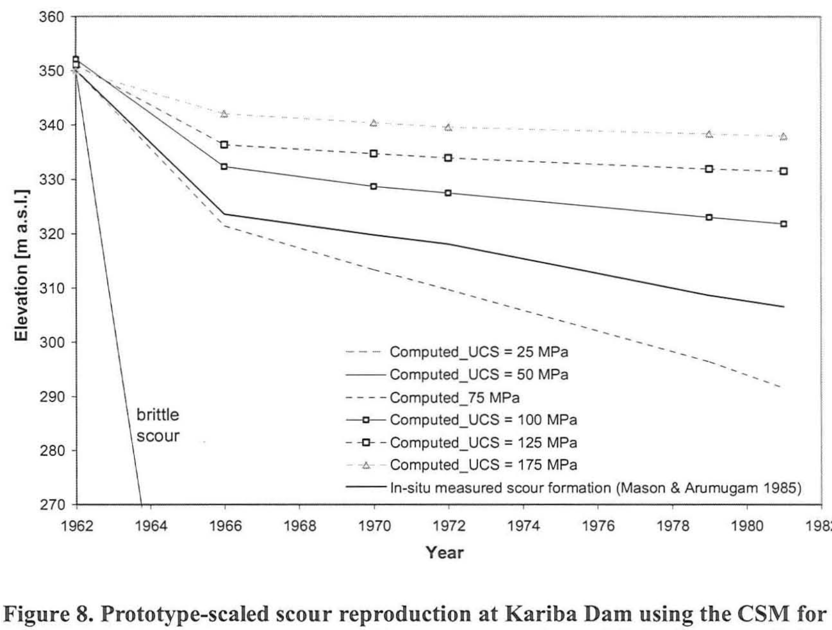

Figure 8. Prototype-scaled scour reproduction at Kariba Dam using the CSM for different UCS strengths (Bollaert, 2005) and comparison with in-situ scour hole.

APPLICATION TO FOLSOM DAM (US)

The DI and CFM modules have been applied to the lined stilling basin of Folsom Dam, a concrete gravity dam with a height of about 100 m situated near Sacramento, California, US. Due to a significant increase of the initial PMF estimates, the outlet works of the dam were initially proposed to be increased. This would have resulted in a significant increase of turbulent pressure fluctuations impacting the concrete lining of the downstream stilling basin.

Hence, at first, a concrete lining stability study has been performed, pointing out the need for significant additional steel anchors to keep the slabs in place. Following this, a rock scour study has been performed of the fractured rock mass underneath the concrete lining, to check for scour formation and extent under extreme conditions and following potential lining failure. In the following, examples are provided of results that were generated for the PMF event (Bollaert et al., 2006).

Figure 9 presents a plan and perspective view of the final 3D shape of the scour hole through the rocky foundation of the stilling basin. One can easily detect the areas of impact of the jets issuing from the outlets. The model predicts 6-9 m of scour formation within the first 12-24 h of a PMF flood, while subsequent scour deepening would need far more time to occur. No scour forms at the toe of the dam.

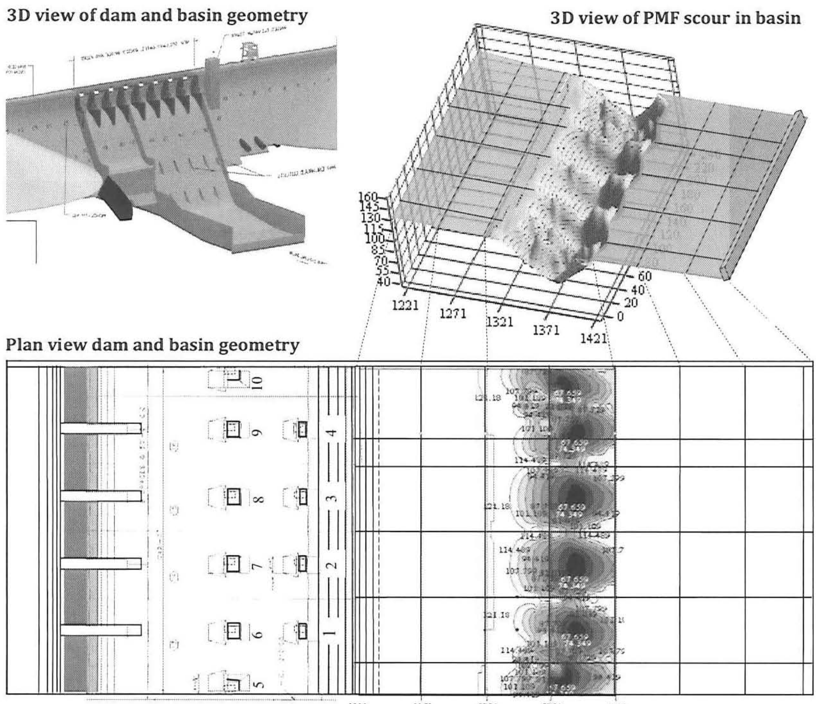

Figure 9. Plan view and perspective view of scour contours in stilling basin due to upper tiers functioning.

APPLICATION TO TUCURUI DAM (BRAZIL)

Tucurui Dam Spillway is located on the Tocantins River in northern Brazil. The spillway is characterized by an ogee type gate-controlled structure topped by 23 radial gates (20.75m high x 20m wide), a compact flip bucket and a 50m deep plunge pool (Figure 10). The design discharge is 110,000 cms under a gross head of 60 to 70 m. Hydraulics laboratory model tests resulted in the forecast of a satisfactory scouring behavior for a pre-excavated plunge pool at an elevation of – 40 m a.s.l.

Scour formation in the downstream plunge pool has been described by a series of bathymetric surveys since 1984. These showed that, as predicted by the laboratory tests, the maximum observed scour depth was of only 5 m. It was assumed that this erosion is related to removal of partially detached rock blocks during initial spillage. These blocks were fractured and detached by blasting during dam construction.

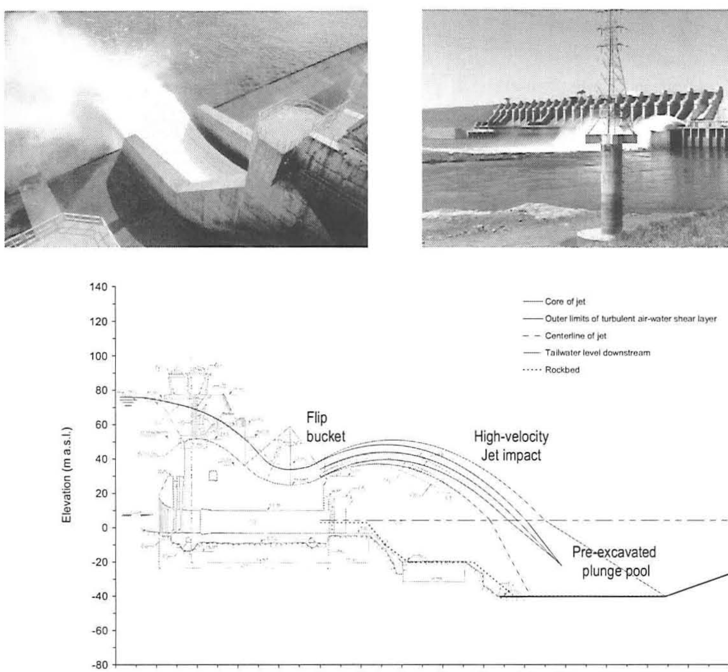

Figure 10. Photos and longitudinal section of spillway at Tucurui Dam.

Hence, it may be stated that the pre-excavated plunge pool behaves like expected during dam construction. For a recorded period of 17 years, incorporating 6 flood events of more than 31'000 m^3/s and a maximum value of 43'400 m^3/s, no significant scour formation could be observed.

The CSM model has first of all been calibrated based on the assumption that, for flood events of up to 50'000 m^3/s, no significant scour forms at the plunge pool bottom. Second, the model has been applied to a fictitious design flood event with a discharge of 110'000 m^3/s (Bollaert & Petry, 2006).

Comprehensive Fracture Mechanics (CFM) results

By using realistic parametric assumptions regarding rock resistance to scour, scour formation down to a plunge pool bottom level of about – 54.9 m (= 14.9 m of additional scour depth) has been computed for a design flood duration of 2 months.

Second, for 8 months of design flood, the corresponding plunge pool scour elevation is at -56.5 m (= 16.5 m of additional scour depth). Finally, on the long term (= after 80 months of design flood), a maximum scour elevation of -59.2 m has been computed (= 19.2 m of additional scour depth). In other words, even during very long periods of design discharge at Tucurui Dam, potential scour formation would still remain within controllable limits.

Dynamic Impulsion (DI) results

Computed scour becomes more important than for the CFM model, with scour at – 63 m for beneficial rock resistance assumptions and down to – 94 m for conservative rock resistance assumptions. For average (most reasonable) parametric assumptions, scour goes down to – 79 m, i.e. 39 m of additional scour depth.

Nevertheless, it has to be kept in mind that the DI model results largely depend on the assumed ratio of rock block height to side length. Under conservative assumptions, this ratio has been taken equal to 0.5. Under average assumptions, this ratio has been taken equal to 0.75. Using the DI method also means that only completely detached rock blocks would be present at depth in the plunge pool bottom, which is most probably not the case.

APPLICATION TO KARAHNJUKAR DAM (ICELAND)

Landsvirkjun, the National Power Company in Iceland, has completed in 2008 the 690 MW HEP Kárahnjúkar project in eastern Iceland. The main dam is a 200 m high CFRD dam. The bottom outlet of Kárahnjúkar Dam is 5.2 m wide, 6 m high and is concrete lined (Figure 11).

The first 50 m are near horizontal, followed by a slope change down to 5 % for the remaining 300 m. The invert and side walls are concrete lined up to a height of 3.5 m. The tunnel ends with a double curvatured flip bucket that projects the water jet with an angle between 21 and 28° into the downstream canyon.

Numerical computations have been performed of potential scour formation of the canyon following bottom outlet operation. Both downstream tailwater level and duration of discharge have been accounted for. The results show that scour formation in the canyon riverbed will remain limited (Figure 12). Scour may occur under the form of uplift and displacement of loose blocks that are already present at the riverbed. Subsequent fracturing and block formation of the in-situ rock mass will take considerable time to occur and will most probably not result in excessive scour formation.

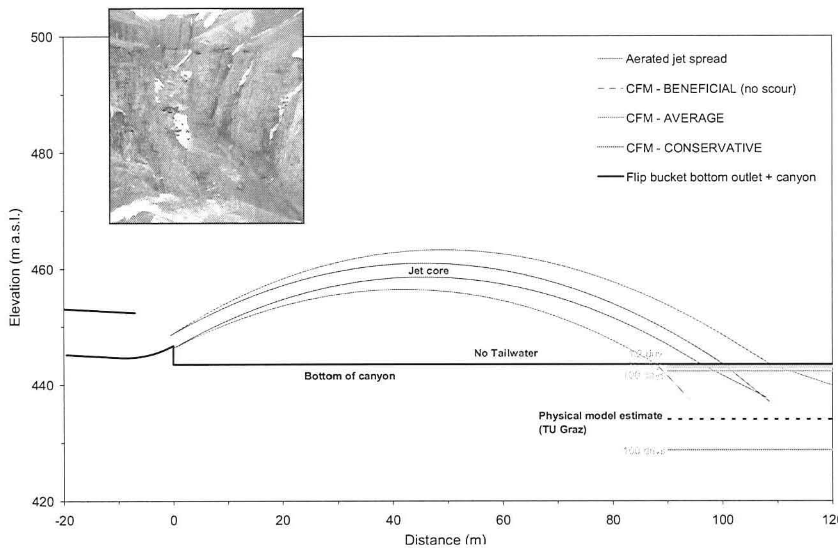

Figure 11. Scour formation in canyon as predicted by CFM module.

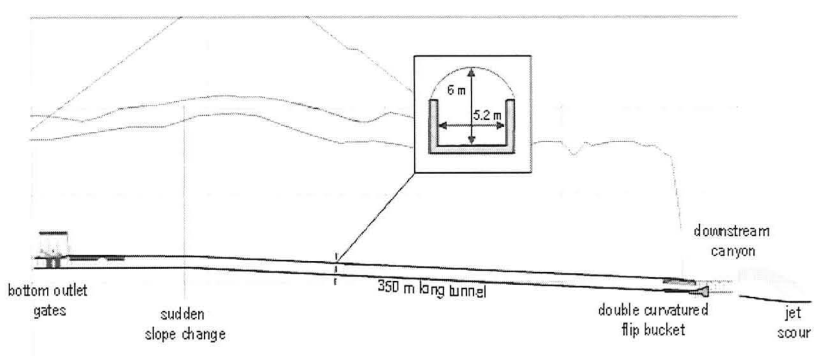

Figure 12. Longitudinal profile of bottom outlet and flip bucket.

CONCLUSIONS

Sound assessment of the physical processes responsible for rock mass failure at high-head dams and plunge pools has shown the importance of air bubbles present in the water. The bubbles do not only influence the jet during its fall and the diffusion of the jet through the pool and the pressure fluctuations it generates, but also govern the cyclic pressure waves of the water inside the underlying rock joints. As such, the bubbles are directly relevant to hydraulic jacking of the rock mass.

Furthermore, a large series of near-prototype scaled laboratory tests have shown that use of small scale physical models may significantly alter the outcome of scour depth predictions. Especially flow turbulence and jet and pool aeration should be correctly reproduced in order to obtain sound scour predictions. The complex three-phase behavior of fractured rock impacted by turbulent pressures cannot be reproduced on a small scale model.

Hence, based on a sound analysis of the multi-phase physics of rock failure mechanisms and a large series of near-prototype scaled laboratory recordings of water pressures in artificially generated rock joints, a numerical scour prediction model has been developed. The model predicts scour formation in any type of fractured medium by computing fracture propagation, dynamic uplift and peeling off of blocks.

Appropriate calibration of the model needs the assessment of a number of hydraulic, hydrologic, geometric and geomechanic parameters. Especially the time duration and average discharge values of floods, the intrinsic rock mass strength and the initial degree of fracturing of the rock mass have to be known in a sufficiently precise manner to obtain values that can be used for practice.

When these values are available or can be reasonably estimated based on in-situ observations or based on values from similar dam sites, the numerical model can be used to predict further scour formation as a function of time and/or to evaluate the ultimate scour depth on the long term.

During the last 10 years, the model has been widely used for scour prediction and/or mitigation at high-head dams and in stilling basins. Within this framework, based on historic floods and observed scour formation, the numerical model could be calibrated and thus used to predict potential future scour formation with time. Feedback from practice has shown that the model provides significant insight into the different rock failure mechanisms and is able to assist the engineer when designing scour mitigation measures.

REFERENCES

Bollaert, E.F.R. (2002). "Transient water pressures in joints and formation of rock scour due to high-velocity jet impact." *PhD Thesis N°2548*, Ecole Polytechnique Fédérale de Lausanne, Switzerland.

Bollaert, E.F.R. (2004). "A comprehensive model to evaluate scour formation in plunge pools." *Int. Journal of Hydropower & Dams*, 2004(1), pp. 94-101.

Bollaert, E.F.R. and Schleiss, A. (2005). "Physically Based Model for Evaluation of Rock Scour due to High-Velocity Jet Impact." *J. of Hydr. Eng.*, Vol. 131, N° 3, pp. 153-165.

Bollaert, E.F.R., Vrchoticky, B. and Falvey, H.T. (2006). "Extreme Scour Prediction at High-Head Concrete Dam and Stilling Basin (United States)." *3rd Intl. Scour and Erosion Conference*, Amsterdam, 2006.

Bollaert, E.F.R. & Petry, B. (2006). "Application of a physics based scour predictionmodel to Tucurui dam spillway (Brazil)." *Intl. Symp. On Hydr. Structures*, Ciudad Guyana, Venezuela.

Bollaert, E.F.R., Manso, P. and Schleiss, A.J. (2009). "Discussion of: "Effect of jet aeration on hydrodynamic forces on plunge pool floors." *Canadian Journal of Civil Engineering*, Vol. 36, pp. 524-526.

Council for Scientific and Industrial Research, Report N°EMAS-C 95098 (2001). Foundation for Water Research. UK.

Ervine, D.A. & Falvey, H.R. (1987). "Behavior of turbulent jets in the atmosphere and in plunge pools." *Proceedings of the Institution of Civil Engineers, Part 2*, Vol. 83, pp. 295-314.

Federspiel, M., Bollaert, E.F.R. and Schleiss, A. (2009). "Response of an intelligent block to symmetrical core jet impact." *Proceedings of the 33rd Congress of IAHR, ISBN: 978-94-90365-01-1*, Vancouver, Canada, 9.-14. August 2009, CD-Rom, 2009, pp. 3573-3580.

Manso, P., Bollaert, E.F.R. and Schleiss, A.J. (2006). "Impact pressures of turbulent high-velocity jets plunging in pools with flat bottom." *Experiments in Fluids*.

Mason, P.J. and Arumugam, K. (1985). "A Review of 20 Years of Scour Development at Kariba Dam." *Int. conf. on the Hydraulics of Floods and Flood Control,* Cambridge, England.

Observational Method for Estimating Future Scour Depth at Existing Bridges

A.V. Govindasamy[1], J.-L. Briaud[2], D. Kim[3], F. Olivera[4], P. Gardoni[5], and J. Delphia[6]

[1]Staff Engineer, Geocomp Corporation, 1145 Massachusetts Avenue, Boxborough, MA 01719; PH (978) 621-8106; email: agovindasamy@geocomp.com
[2]Professor and Holder of the Buchanan Chair, Zachry Dept. Of Civil Engineering, Texas A&M University, College Station, TX 77840; PH (979) 845-3795; email: briaud@tamu.edu
[3]GIS Developer, Dewberry, 8401 Arlington Boulevard, Fairfax, VA 22031; PH (703) 206-0847; email: dokim@dewberry.com
[4]Associate Professor and Head of the Water Resources Division, Zachry Dept. Of Civil Engineering, Texas A&M University, College Station, Texas, 77840; PH (979) 845-1404; email: folivera@civil.tamu.edu
[5]Associate Professor, Zachry Dept. Of Civil Engineering, Texas A&M University, College Station, Texas, 77840; PH: (979) 845-4340; email: pgardoni@civil.tamu.edu
[6]Geotechnical Engineer, Texas Department of Transportation Bridge Division-Geotechnical Branch, Austin, Texas; PH: (512) 416-2359; email: jdelphi@dot.state.tx.us

ABSTRACT

Bridge scour can cause damage to bridge foundations and abutments. Bridges with foundations that are unstable for calculated and/or observed scour conditions are termed scour critical bridges. There are approximately 17,000 scour critical bridges in the United States. This designation comes in part from the use of over-conservative methods that predict excessive scour depths in erosion resistant materials. Other methods capable of overcoming this over-conservatism are uneconomical because they require site-specific erosion testing. This paper proposes a new bridge scour assessment method. The new method, termed Bridge Scour Assessment 1 (BSA 1) is the first part of a three level bridge scour assessment procedure that was developed for the Texas Department of Transportation. It does not require site-specific erosion testing and eliminates the over-conservatism in current methods. BSA 1 uses charts that extrapolate or interpolate measured scour depths at the bridge to obtain the scour depth corresponding to a specified future flood event. The scour vulnerability depends on the comparison between the predicted and allowable scour depths. This paper also includes a new hydraulic-hydrologic analysis procedure for the determination of flow parameters required in the scour analysis. This procedure was developed for the State of Texas, and is economical and reasonably reliable from a hydrologic standpoint. This procedure is versatile as it can be applied to any region with sufficient flow gages. The 11 case histories used to validate BSA 1 showed good agreement between predicted and measured values. BSA 1 was then applied to 16 bridges where 6 out of 10 bridges classified as scour critical by current methods were found to be stable. These indicate that the method allows for more realistic evaluation of bridges for scour

while not requiring site-specific erosion testing. BSA 1 was finalized in April 2009 and six months later has already been used by Texas Department of Transportation engineers to evaluate 350 scour critical bridges in the State of Texas.

INTRODUCTION

Bridge scour is the term describing the loss of geomaterials due to water flowing around bridge supports. Bridge foundations can be undermined if excessive scour takes place, possibly leading to the failure of the bridge. Current standard bridge scour assessment methods in use are either qualitative initial evaluations that can be unreliable or quantitative scour depth evaluations that are overly conservative when applied to erosion resistant materials.

There are approximately 17,000 scour critical bridges in the United States (Pagan-Ortiz 1998). In the State of Texas alone, there are 600 bridges designated as scour critical. This designation comes in part from the use of methods that predict excessive scour depths in erosion resistant materials. This paper presents a quantitative bridge scour assessment method, termed Bridge Scour Assessment 1 (BSA 1) which accounts for time-dependent scour depth using field measurements. This method eliminates the over-conservatism in erosion resistant materials and does not require site-specific erosion testing. BSA 1 is part of a three phase comprehensive bridge scour assessment package which includes maximum scour depth and more detailed time-dependent scour depth calculations in the remaining two phases, termed BSA 2 and BSA 3 (Govindasamy 2009 and Briaud et al. 2009).

This paper deals with local scour, more specifically pier and contraction scour. The contribution of abutment scour towards the total scour depth is not included because it is usually more practical and favorable to protect the abutment with riprap or other scour countermeasures.

CURRENT PRACTICE

Current bridge scour evaluation procedures rely upon three categories of assessment methods. The first category, termed Level 1 analysis, is a preliminary scour evaluation procedure that is based on field observations and is primarily qualitative in nature, but could also rely on simplified scour depth–hydraulic parameter relationships that are mainly based on flume tests in sand. This category does not utilize actual measured scour data. The second and third categories, termed Level 2 and Level 3 analysis, involve more detailed calculations of maximum scour depth based on flume tests in sand. The first method does not provide realistic results in many cases due to its reliance on a more qualitative form of assessment. The second and third methods are often conservative in the case of clays, which are known to erode at a much slower rate than sand.

Preliminary scour evaluation procedures have been developed by or for several state departments of transportation (DOTs). For example, the Montana DOT, in collaboration with the United States Geological Survey (USGS), developed a rapid scour evaluation process that relies upon calculated scour depth– measured hydraulic parameter relationships (Holnbeck and Parrett 1997). A similar method has also been adopted by the Missouri DOT (Huizinga and Rydlund 2004). The Tennessee DOT uses an initial evaluation process that utilizes a qualitative index based on field observations to describe potential scour related problems (Simon et al. 1989). Similar qualitative methods have been adopted by the California, Idaho, and Texas DOTs, and the Colorado Highway Department for their initial assessment of bridges for scour. Johnson (2005) presented a preliminary assessment procedure that individually rates 13 stream channel stability indicators, which are then summed to provide an overall score that places a bridge in one of four categories: excellent, good, fair, and poor (Govindasamy et al. 2008).

Current practice for more detailed scour evaluation is heavily influenced by two Federal Highway Administration (FHWA) hydraulic engineering circulars (HECs) called HEC-18 and HEC-20 (Richardson and Davis 2001, and Lagasse et al. 1995). These circulars have two major categories of bridge scour calculations, termed here as HEC-18 Sand and HEC-18 Clay. The HEC-18 Sand method in known to be overly conservative in the case of clays and some rocks because it is based on flume tests in sand and essentially estimates the maximum (or equilibrium) scour depth, Z_{max} that can occur at the bridge. It does not account for time-dependent scour, Z_{final}. The HEC-18 Clay method (Briaud et al. 1999 and Briaud et al. 2005) consists of pier and contraction scour models that are capable of accounting for time-dependent scour. HEC-18 Clay, previously referred to as the Scour Rate in Cohesive Soils (SRICOS) method requires site-specific erosion testing (Govindasamy 2008).

THE HEC-18 CLAY METHOD

The HEC-18 Clay method predicts the scour depth versus time curve around a cylindrical pier and in bridge contractions in clay. This method was employed in the development of BSA 1. The method involves obtaining soil samples at the bridge site and testing it in the Erosion Function Apparatus or EFA to obtain the erosion function (Briaud et al. 2001a). Further analysis is carried out based on the erosion function to determine the scour depth versus time curve. This curve, representing the time-dependent scour depth is modeled as a hyperbola with the initial rate of scour as the initial slope and Z_{max} as the asymptotic value of the hyperbola. The reader is referred to Briaud et al. (1999) and Briaud et al. (2005) for detailed descriptions of HEC-18 Clay.

BRIDGE SCOUR ASSESSMENT 1 (BSA 1)

The main idea behind BSA 1 is that the best information available for existing bridges including scour critical bridges is not equations and calculations but the observations at the bridge site and that these observations can be extrapolated or interpolated to predict the scour depth under a major flood in the future. More specifically, the scour depth corresponding to a specified future flood event can be obtained from scour depth observations at the site and from charts that relate the future scour depth ratio (Z_{fut}/Z_{mo}) to the future velocity ratio (V_{fut}/V_{mo}). Here, Z_{fut} is the scour depth corresponding to a specified future flood, Z_{mo} is the maximum observed scour at the bridge, V_{fut} is the velocity corresponding to the specified future flood, and V_{mo} is the maximum velocity observed at the bridge until the time Z_{mo} is measured. These charts are termed the Z-Future Charts (Govindasamy 2009 and Briaud et al. 2009). The scour vulnerability of the bridge depends on the comparison between Z_{fut} and the allowable scour depth of the foundation, Z_{thresh}. V_{fut}/V_{mo} is obtained through a simplified hydrologic analysis that is presented later in this paper and answers the question: "what is the highest flood that this bridge has seen since its construction?" BSA 1 consists of two flowcharts, i.e. the BSA 1 (Uniform Deposit) and BSA 1 (Multilayer Analysis) flowcharts. BSA 1 (Uniform Deposit) shown in Figure 1 is for a bridge site that is underlain by a uniform deposit or for a scour depth being investigated that is not expected to exceed the top layer of a multilayer deposit. BSA 1 (Multilayer Analysis) is used for layered deposits when the scour depth being investigated penetrates beyond the top layer. BSA 1 (Multilayer Analysis) is beyond the scope of this paper. The reader is referred to Govindasamy (2009) and Briaud et al. (2009) for a detailed description of the method.

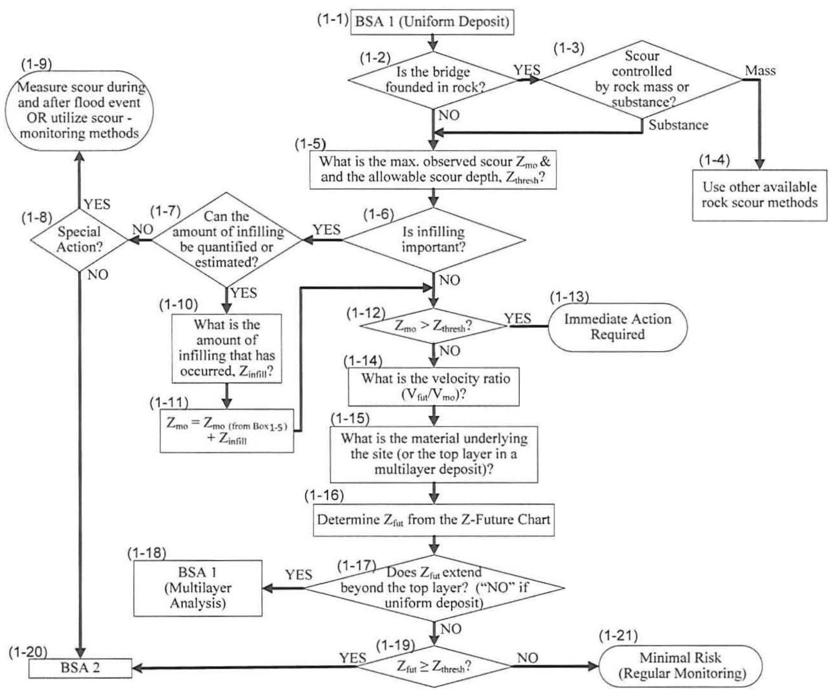

FIGURE 1 BSA 1 (Uniform Deposit) Flowchart.

The Z-Future Charts

To develop the Z-Future Charts, HEC-18 Clay simulations were carried out by employing an equivalent time to represent the age of the bridge, varying the pier and contraction scour parameters, and the material underlying the bridge site. The concept of equivalent time was developed for pier and contraction scour by (Briaud et al. 2001b and Wang 2004), who define it as the time required for the maximum velocity in the hydrograph to create the same scour depth as the one created by the complete hydrograph. This concept was needed to enable a large number of simulations to be carried out through more simple calculations rather than complex hydrograph based analysis. The materials underlying the site are in accordance with five of six erosion categories in that are presented in what is termed the Erosion Function Chart (Figure 2) (Govindasamy 2009 and Briaud 2008). These simulations computed the time-dependent scour depth as a result of two consecutive flows having velocities V_{mo} and V_{fut}, respectively.

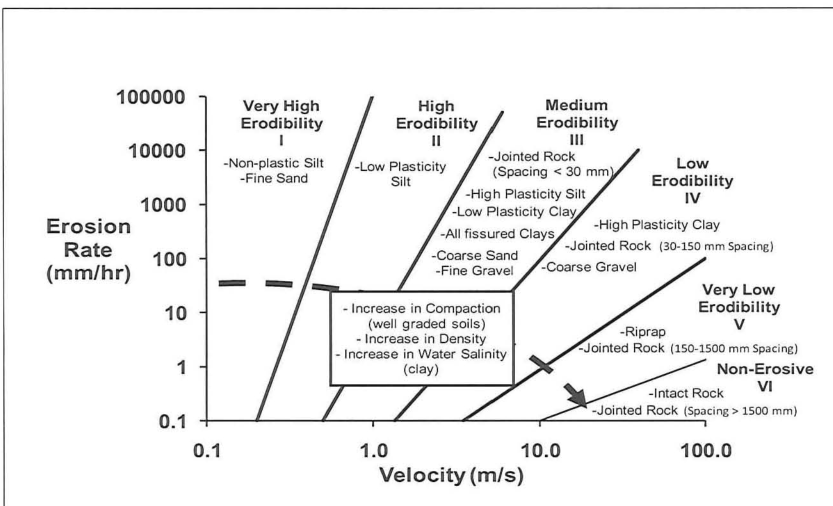

FIGURE 2 The Erosion Function Chart.

The material categories involved in these simulations are Erosion Categories I through V. Category VI was omitted from the simulations since materials that fall under this category are non-erosive.

HEC-18 simulations for pier and contraction scour employing the equivalent time concept described above were carried out by creating various combinations of the following parameters:

- V_{fut} and V_{mo} ranging from 0.3 ft/s (0.1 m/s) to 11.5 ft/s (3.5 m/s), which is well within the velocity range of flow in most rivers;
- Upstream water depth, H_1, ranging from 16.4 ft (5 m) to 65.6 ft (20 m);

- Channel contraction ratio, R_c, which is the ratio of the contracted channel width to the uncontracted channel width, ranging from 0.5 to 0.9;
- Soil-critical velocity, V_c, according to the five material categories investigated;
- Pier diameter, D, ranging from 0.3 ft (0.1) m to 32.8 ft (10.0 m);
- Age of the bridge, t_{hyd}, ranging from 5 years to 75 years.

The simulations provided approximately 360,000 combinations of the above parameters for each material category and age of the bridge. The Z-Future Charts resulting from this is shown in Figure 3. The data points on the figure have been omitted to improve the clarity of the curves. The curves are essentially upper bound envelopes of the data points from the simulations. The reader is referred to (Govindasamy 2009 and Briaud et al. 2009) for the data points. The Z_{fut} values were normalized with the corresponding Z_{mo} values, and the V_{fut} values were normalized with the corresponding V_{mo} values and subsequently plotted against each other to form the Z-Future Charts.

For the case of Category I and II materials, two ranges of pier diameter (0.1 m to 1.0 m and 1.0 m to 10 m) are represented by two curves in the same figure (Figure 3(a)). For the case of Category III materials, the Z-Future Charts were separated into two charts, i.e., one for D ranging from 0.1 m to 1.0 m and the other for D ranging from 1.0 m to 10.0 m (Figures 3(b) and 3 (c)). This was done due to notable difference in Z_{fut}/Z_{mo} ratios from these two ranges of pier diameters. The pier diameters for all other categories were lumped together, i.e., ranging from 0.1 m to 10.0 m since there was no significant difference due to the low erosion rates.

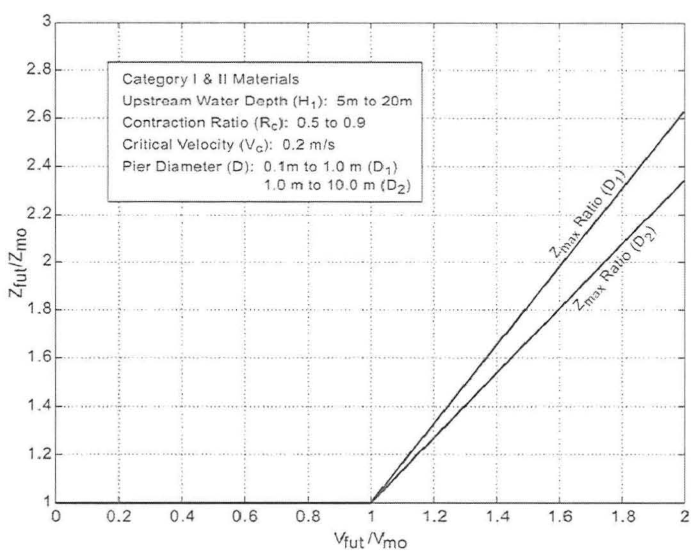

FIGURE 3(a) Z-Future Chart for Category I & II Materials

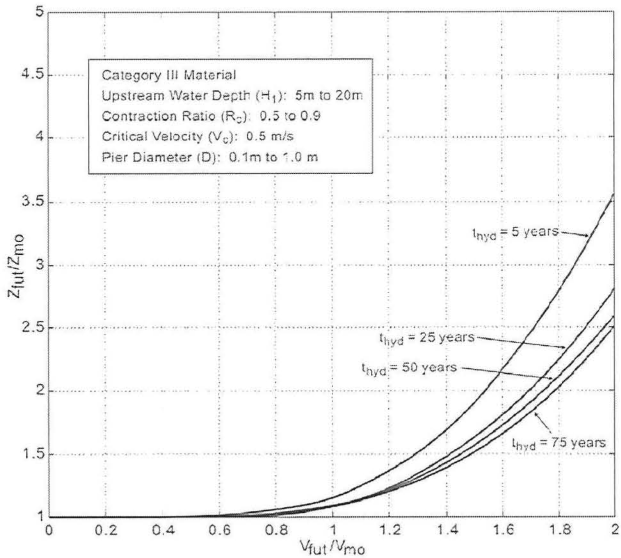

FIGURE 3(b) Z-Future Chart for Category III Materials (Pier diameter: 0.1 m to 1.0 m).

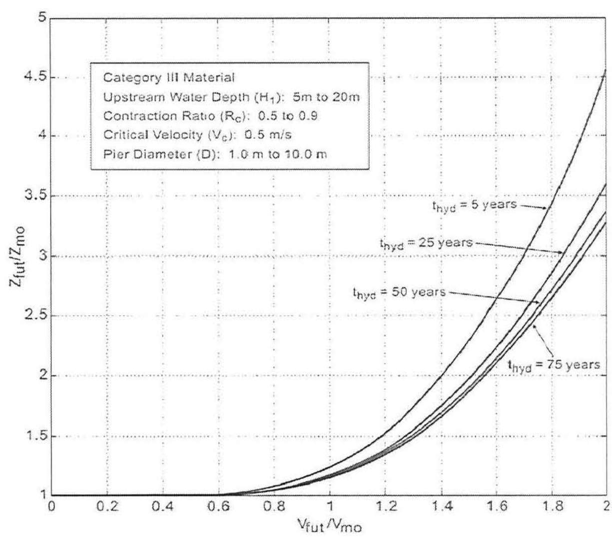

FIGURE 3(c) Z-Future Chart for Category III Materials (Pier diameter: 1 m to 10 m).

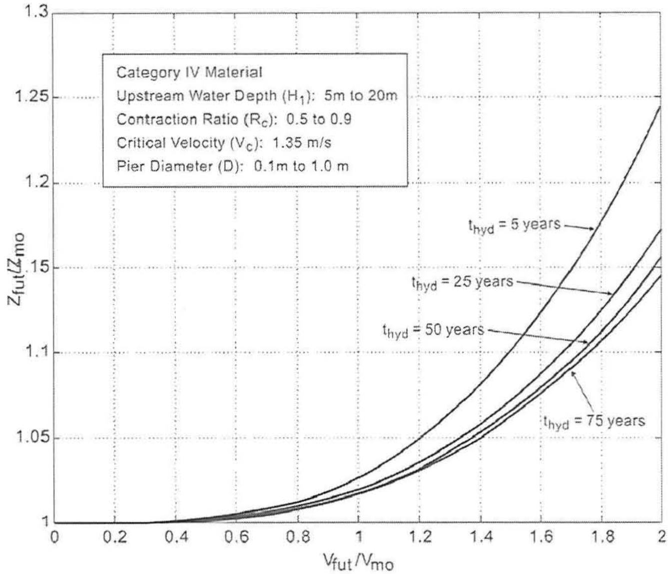

FIGURE 3(d) Z-Future Chart for Category IV Materials.

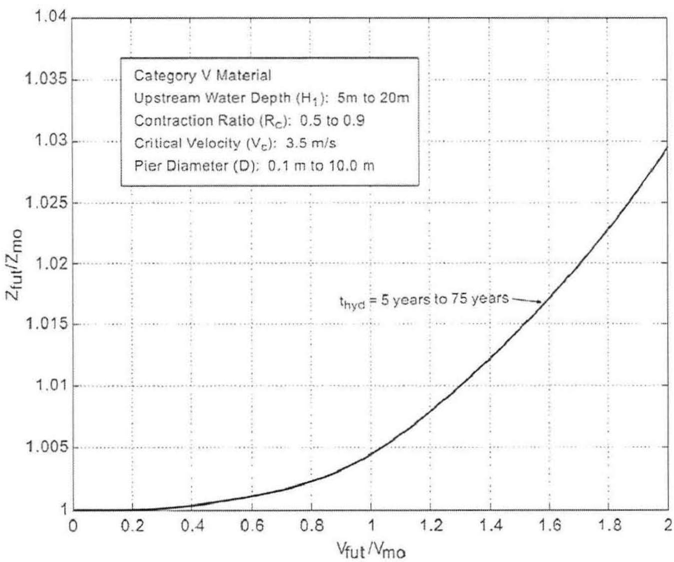

FIGURE 3(e) Z-Future Chart for Category V Materials.

In general, the Z-Future Charts lead to the determination of Z_{fut} by employing the following relationship:

$$Z_{fut} = Z_{mo} \times f\left(V_{fut}/V_{mo}\right) \qquad (1)$$

where f is some function of (V_{fut}/V_{mo}) obtained from the Z-Future Charts and is always equal to or greater than unity (for the case of clear-water scour, as considered in these simulations). The velocity ratio (V_{fut}/V_{mo}) is plugged into the chart by the user to obtain the value of the function f, based on the material type, age of the bridge, and pier scour and contraction scour parameters. Z_{mo} is obtained from bridge inspection and measurement records.

The BSA-1 Procedure and Flowchart

The BSA-1 flowchart is shown in Figure 1. The first step in BSA 1 is to identify whether the bridge is founded in rock or not. If the bridge is founded in rock, BSA 1 then separates rock mass and rock substance–controlled erosion. Rock mass–controlled erosion occurs when reactions of rock materials to hydraulic stress are controlled by rock mass properties such as fracture and joint spacing, bedding planes, folding, and spatial orientation (Cato 1991). In rock mass–controlled erosion, the rock materials are eroded and transported as blocks. Rock substance–controlled erosion is the erosion process that is governed by the property of the mineral grains forming the rock. In BSA 1 (Uniform Deposit), scour assessments of rock materials that undergo rock mass–controlled erosion should use other rock scour assessment methods. Rock materials that undergo rock substance–controlled erosion are treated as soils in BSA 1.

As mentioned above, the Z-Future Charts were developed based on clearwater conditions. However, if live-bed scour has taken place, the depth of the scour hole measured during bridge inspections could be the scour depth after infilling has occurred. This would be the case if the bridge inspection is carried out either during the falling stage of the flood or after the flood event altogether. Since the Z-Future Charts are developed for clear water scour conditions, if the measurements taken during the bridge inspection do not account for possible infilling, Z_{fut} would be under-predicted, as implied by Equation (1). This would therefore lead to an unconservative or even erroneous assessment of the bridge for scour. Several options are available in BSA 1 when infilling is expected to occur:

1. Quantifying the amount of infilling that has occurred, Z_{infill}. This can be done, for example by using engineering judgement and local experience, performing sediment transport calculations, model tests, or probing into the scour hole to roughly identify the extent of the infilled material. In this case, the value of Z_{mo} used in Equation (1) is the summation of the measured scour depth and Z_{infill}.
2. Taking special actions such as measuring the scour depth during and after flood events or utilizing scour-monitoring methods.
3. Carrying out BSA 2 or BSA 3, which are beyond the scope of this paper.

If the site is underlain by a multilayer deposit and Z_{fut} extends beyond the top layer, then BSA 1 (Multilayer Analysis) as presented in Govindasamy (2009) and Briaud et al. (2009) should be carried out. Otherwise, if the site is underlain by a uniform deposit or if Z_{fut} does not extend beyond the top layer in a multilayer deposit, BSA 1 (Uniform Deposit) is continued. If Z_{fut} is equal to or greater than the allowable scour depth, Z_{thresh}, BSA 2 should be undertaken. Otherwise, the bridge is deemed "minimal risk" and should undergo regular monitoring. However, if the bridge does experience a major flood, for example the 100-year flood, BSA 1 should be carried out again soon after to assess the bridge for a future flood after having undergone the major flood.

HYDRAULIC AND HYDROLOGIC ANALYSIS FOR BSA 1

The required hydraulic information for BSA 1 is V_{fut}/V_{mo}. From this point forward, the term V_{100} will substitute the term V_{fut} when the future flood event is specifically considered as the 100-year flood. There are two cases pertaining to the availability of flow gages (flow data) when estimating V_{fut}/V_{mo}, i.e. when flow data is available or unavailable at the bridge.

Obtaining the velocity ratio when flow data is available at the bridge being assessed for scour

In this case, the hydraulic information required for BSA 1 can be determined in a fairly straightforward manner as follows:

1. Obtain the time series of annual instantaneous flow peaks at the bridge location.
2. Perform flood frequency analysis (FFA) on unregulated flow records to obtain the flow corresponding to the 100-year flood, Q_{100}.
3. Determine the maximum flow value from the time series ignoring data recorded before the bridge was constructed. This flow value is the maximum flood experienced by the bridge Q_{mo}.
4. Convert Q_{100} and Q_{mo} into V_{fut} and V_{mo}, respectively using typical hydraulic analysis tools such as HEC-RAS. The software TAMU-FLOW, which models the relationship between the discharge and velocity in uniform flow, was developed for this study. TAMU-FLOW is simpler to use than HEC-RAS and is available from the authors at no cost.
5. Calculate V_{100}/V_{mo}.

Obtaining the velocity ratio when flow data is unavailable at the bridge being assessed for scour

In this case, V_{fut}/ V_{mo} should be inferred. This paper introduces a method which utilizes flow data collected at gages near the bridge being investigated. V_{fut}/ V_{mo} is determined as follows:

1. Obtain Q_{mo} and it's corresponding recurrence interval RI_{Qmo} at the nearby gages
2. Obtain RI_{Qmo} at the bridge being assessed for scour by spatially interpolating RI_{Qmo} observed at the nearby gages. This procedure is addressed in the proceeding section.

3. Obtain Q_{100}/Q_{mo} using the relationship between RI_{Qmo} and Q_{100}/Q_{mo} developed for this study (Figure 4). The development of the RI_{Qmo} - Q_{100}/Q_{mo} relationship is presented in a proceeding section.
4. Convert Q_{100}/Q_{mo} into V_{100}/V_{mo} using Manning's equation.

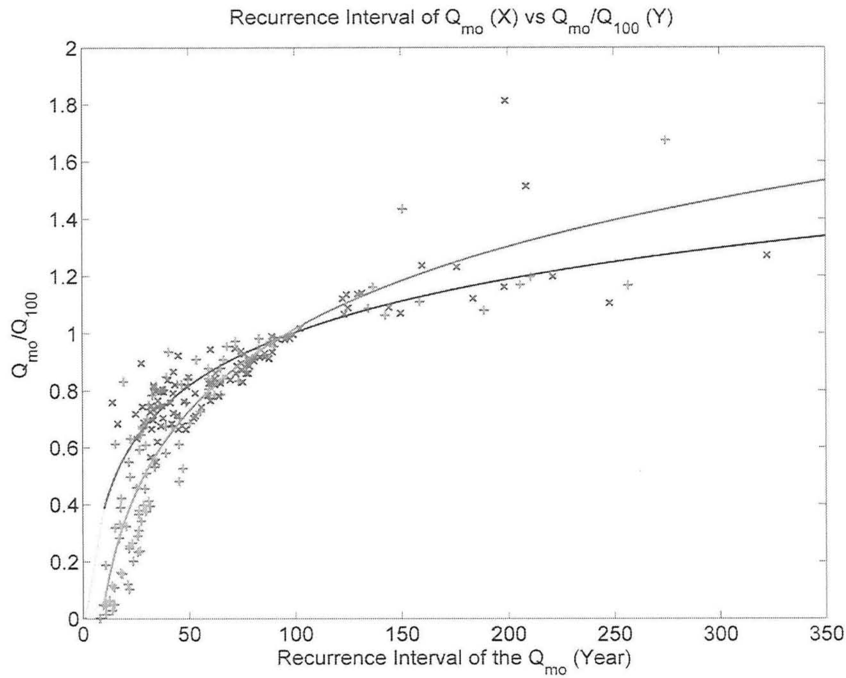

FIGURE 4 Relationship between recurrence interval of the Maximum Flow Peak and Q_{mo}/Q_{100}.

Estimation of the recurrence interval of the maximum flow at bridge being assessed without flow data

The steps to determine the recurrence interval of Q_{mo} at the bridge being assessed for scour is as follows:

1. Obtain the yearly flow peak data from flow gages that are close to the ungaged basin of concern, i.e. where the concerned bridge without flow data is located.
2. Perform FFA for all those gages to obtain the recurrence interval of the yearly instantaneous peak flow (YIPF) at all gage locations during the years of concern (i.e., starting from the year in which the bridge was built to the year of the most recent bridge inspection).

3. For each year, spatially interpolate the recurrence interval of YIPF for the nearby gages to obtain the recurrence interval at the bridge being assessed for scour. Here, a linear interpolation method is used.
4. Obtain RI_{Qmo} at the bridge being investigated during the period of concern by choosing the highest recurrence interval calculated in the preceding step during the specified period.

This procedure has been automated for the State of Texas in the software tool TAMU-FLOOD which was developed specifically for this study. TAMU-FLOOD is available from the authors at no cost. A snapshot of the software output is provided in Figure 5. Figure 5(a) shows the recurrence interval values of the flow peaks observed at flow gages for a given year while the inset shows the corresponding color shading resulting from the interpolation between gages. Figure 5(b) shows the color shaded recurrence interval between a specified time period, in this case between 1970 and 2006. This represents a scour assessment carried out in 2006 at a bridge that was built in 1970.

Relationship between the Recurrence Interval of the Maximum Flow Peak RI_{Qmo} and Q_{mo}/Q_{100}

The RI_{Qmo} - Q_{mo}/Q_{100} relationship shown in Figure 4 is based on data from 101 USGS flow gages across Texas. The reader is referred to Briaud et al. (2009) for details of these gages. For each gage, FFA was performed to obtain the recurrence interval of the maximum yearly peak discharge and also Q_{100}. In Figure 4, Q_{mo}/Q_{100} is plotted against the recurrence interval of the maximum observed flow at each station. The scatter of cross (x) signs results from FFA that was carried out using the generalized extreme value distribution and L-moments method (GEV-LMOM). The scatter of plus signs (+) results from FFA using the generalized extreme value distribution and maximum likelihood method (GEV-MLE). Detailed descriptions on GEV-LMOM and GEV-MLE are given in Hosking and Wallis (1997).

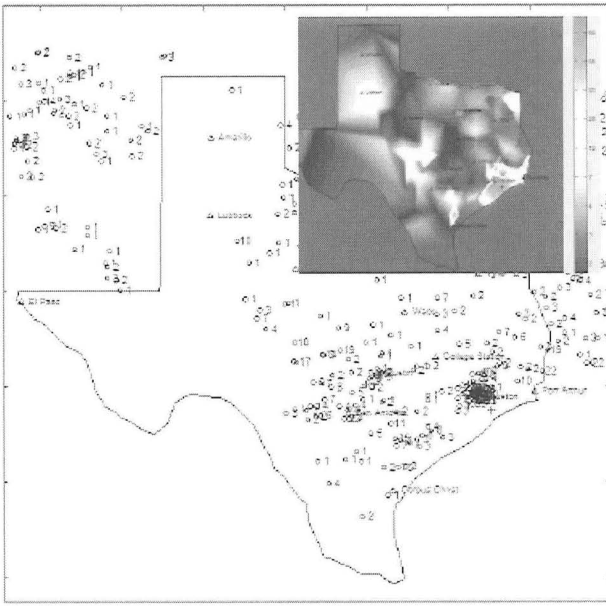

(a)

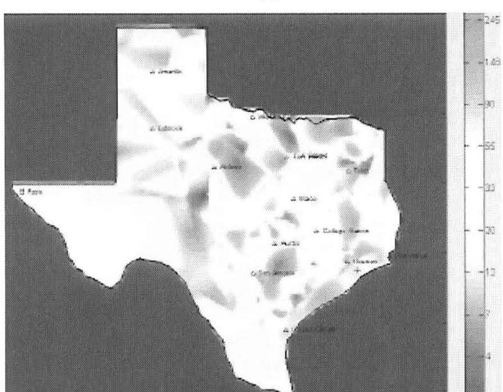

(b)

FIGURE 5 TAMU-FLOOD Output.

In Figure 4, the relationship between the two variables is apparent with R^2 of 0.71 (GEV-LMOM) and 0.83 (GEV-MLE). Thus, this study suggests the following regression equations to obtain the ratio Q_{mo}/Q_{100} from the recurrence interval estimated from the maximum flow peak:

When GEV-LMOM is preferred:

$$\frac{Q_{mo}}{Q_{100}} = 0.4141\ln(RI_{Qmo}) - 0.89, \text{ if } RI_{Qmo} > 10 \tag{2}$$

$$\frac{Q_{mo}}{Q_{100}} = \frac{0.0635}{9}(RI_{Qmo}-1), \text{ if } RI_{Qmo} \leq 10 \tag{3}$$

When GEV-MLE is preferred:

$$\frac{Q_{mo}}{Q_{100}} = 0.2682\ln(RI_{Qmo}) - 0.2315, \text{ if } RI_{Qmo} > 10 \tag{4}$$

$$\frac{Q_{mo}}{Q_{100}} = \frac{0.3861}{9}(RI_{Qmo}-1), \text{ if } RI_{Qmo} \leq 10 \tag{5}$$

In Equations (2) through (5), RI_{Qmo} is the recurrence interval of YIPF. Equations (2) and (4) can yield negative values of Q_{mo}/Q_{100} for small recurrence intervals (i.e., less than 2 years). To prevent this, the portion of the equation that yields the negative recurrence interval was linearly interpolated and presented as Equations (3) and (5).

Q_{mo}/Q_{100} is then converted into V_{100}/V_{mo} using Manning's equation. This can be done without knowing explicit values of V_{mo} and V_{100}. The relationship between Q_{mo}/Q_{100} and V_{100}/V_{mo} using Manning's equation is as follows:

$$\left[\frac{Q_1}{Q_2}\right]^{\frac{1}{4}} < \frac{V_1}{V_2} < \left[\frac{Q_1}{Q_2}\right]^{\frac{2}{5}} \tag{6}$$

The derivation of Equation (6) can be found in Briaud et al. (2009). The choice of the exponent (0.25 - 0.4) can be made based on the shape of the channel cross section. If the flow depth is small compared to the width, an exponent that is close to 0.4 can be used. If the flow depth is large compared to the width, an exponent close to 0.25 can be adopted. Most rivers fall in the category of wide and shallow, and an exponent of 0.35 may be a reasonable approximation on average.

Validation of method to obtain flow parameters

To investigate if the estimated ratio V_{mo}/V_{100} is close to the observed ratio V_{mo}/V_{100}, an approach called cross-validation was used and is as follows:

1. Obtain the recurrence interval of an observed flood at a gage.

2. Assume the flow gage is nonexistent and estimate the recurrence interval at the gage by spatially interpolating observed data from nearby gages. This value is the cross-validated recurrence interval (CVRI).
3. Calculate Q_{mo}/Q_{100} for both the observed and cross-validated recurrence intervals using Equations (2) through (5).
4. Convert Q_{mo}/Q_{100} into V_{mo}/V_{100}.
5. Compare V_{mo}/V_{100} from the observed recurrence interval and CVRI.

A match between the observed and cross-validated values would indicate spatial tendency. The cross validation of V_{mo}/V_{100} was performed for all observed flow peaks in Texas between 1950 to 2006, involving 27,070 flow peaks. Among these, the ones observed at gages that were within 120 miles from other gages were chosen for further analysis (a total of 3845 flow peaks). This filtering criterion was used because even the largest storm observed at one location in a given year has a limited spatial coverage, which was assumed to be 120 miles in this study. The result of the cross validation is shown in Figure 6(a). The correlation coefficient between the two variables is 0.61 indicating that V_{mo}/V_{100} at the bridge location without a flow gage can be predicted, with a certain degree of accuracy from a hydrologic sense by spatially interpolating the results from the gages within this distance. The slope and the intercept of the regression equation was 0.58 and 0.2, respectively. The 1:1 line and the regression equation meet when V_{mo}/V_{100} equals 0.45. This suggests that the predicted V_{mo}/V_{100} greater than 0.45 is generally under-estimated, and vice versa.

Figure 6(b) shows the histogram of the error between the cross-validated and observed velocity ratio. The histogram was produced to quantify the level of error inherent in the suggested approach. The discrepancy between the two variables is distributed in a bell shape with mean, $\mu = -0.04$ and standard deviation, $\sigma = 0.18$. Assuming that the error is normally distributed, the predicted V_{fut}/V_{mo} using the suggested approach would be such that:

$$P\left[\mu-\sigma < \frac{V_{mo}}{V_{100\,(obs)}} - \frac{V_{mo}}{V_{100\,(CV)}} < \mu+\sigma\right] = P\left[-0.22 < \frac{V_{mo}}{V_{100\,(obs)}} - \frac{V_{mo}}{V_{100\,(CV)}} < 0.16\right] = 0.68 \tag{7}$$

$$P\left[\mu-2\sigma < \frac{V_{mo}}{V_{100\,(obs)}} - \frac{V_{mo}}{V_{100\,(CV)}} < \mu+2\sigma\right] = P\left[-0.40 < \frac{V_{mo}}{V_{100\,(obs)}} - \frac{V_{mo}}{V_{100\,(CV)}} < 0.32\right] = 0.95 \tag{8}$$

The uncertainty analysis of the suggested approach presented in Figure 6 would help the user in employing engineering judgment when using the method. For example, Figure 6 and Equation 7 suggest that if the calculated (V_{mo}/V_{100}) is 0.5, the actual (V_{mo}/V_{100}) can range from 0.28 (=0.5-0.18-0.04) to 0.64 (=0.5+0.18-0.04) with ~70% confidence.

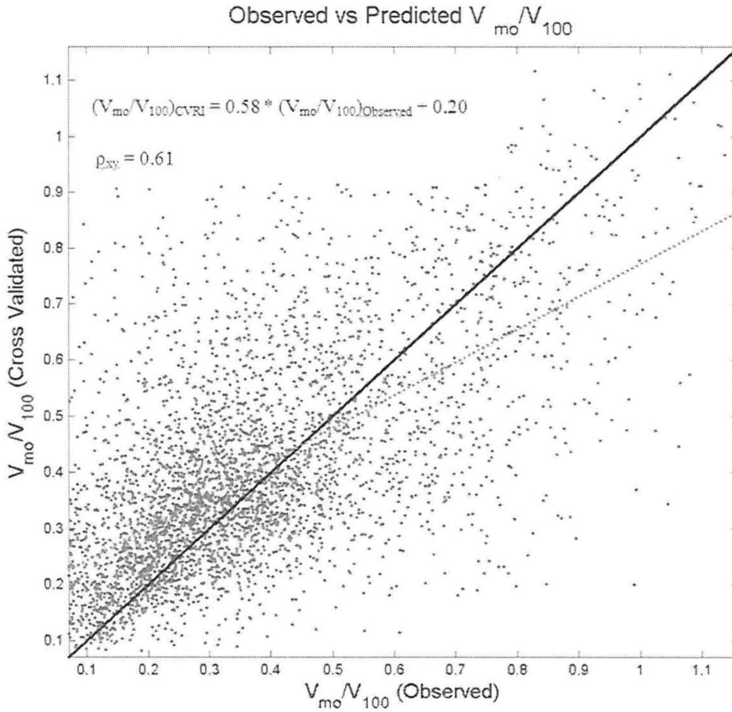

(a)

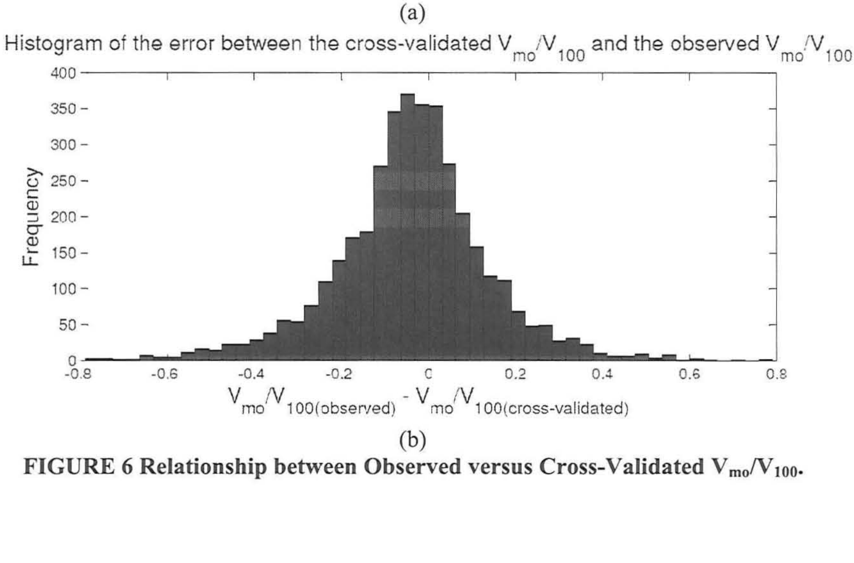

(b)

FIGURE 6 Relationship between Observed versus Cross-Validated V_{mo}/V_{100}.

VALIDATION OF BSA 1

The validation of BSA 1 is aimed at evaluating how well results of BSA 1 match actual field measurements. This is performed by using both flow records and scour measurements at a particular case history bridge. The underlying concept behind the validation procedure is to go back in time and perform a BSA 1 analysis at the bridge and predict a future scour depth value Z_{fut} for a specified time in the future that coincides with when an actual measurement was taken. The validation is simply a comparison between Z_{fut} obtained through BSA 1 at that moment back in time and the actual measurement. In this investigation, nine bridge case histories in Texas were selected for validation. Bridge inspection folders for them were obtained from TxDOT. These were bridges with flow records. In order to carry out a meaningful validation, actual flow records recorded by a suitable flow gage were used. The validation process is summarized as follows:

1. The validation procedure starts at the time the first scour measurement was taken at a particular case history bridge. This time is called T_1 and could represent a particular date, e.g., August 21, 1952, or even a year, say 1952.
2. From the measured velocity time history, the maximum flow velocity experienced by the bridge until T_1, termed V_{mo1}, is obtained. The scour depth measured at the bridge, Z_{mo1}, at time T_1 is obtained from bridge inspection records.
3. A "mock" scour prediction is made at T_1 for a future flood event with velocity V_{fut1} over the next scour measurement interval time, t_{meas1}. It is required that there be actual scour measurements taken at the bridge site at time $T_1 + t_{meas1}$. V_{fut1} is the maximum velocity obtained between T_1 and $T_1 + t_{meas1}$.
4. The Z-Future Chart is then used to obtain the scour depth ratio Z_{fut}/Z_{mo} by using the velocity ratio V_{fut}/V_{mo}. In this case, Z_{mo} is Z_{mo1}, V_{fut} is V_{fut1}, and V_{mo} is V_{mo1}. Z_{fut} is obtained using Equation (1). This Z_{fut} is termed $Z_{fut,predict1}$. Then, $Z_{fut,predict1}$ is compared with the actual measured scour depth, $Z_{fut,meas1}$.
5. Steps 1 through 4 are repeated for the remaining bridge inspection records.

The validation process might yield one or more sets of predicted and measured scour depth for each of the selected bridge case histories. The bridge records had limited bridge scour measurements. In fact, there were no bridge scour measurements taken before the year 1991. Since most of the bridges were reasonably old, they had experienced the largest flow velocity prior to the first bridge scour measurement. This resulted in all the cases having a V_{fut}/V_{mo} ratio of equal to or less than unity. Results of the validation are shown in Figure 7 where they are plotted against the equal value line. There appears to be good agreement between predicted and measured values.

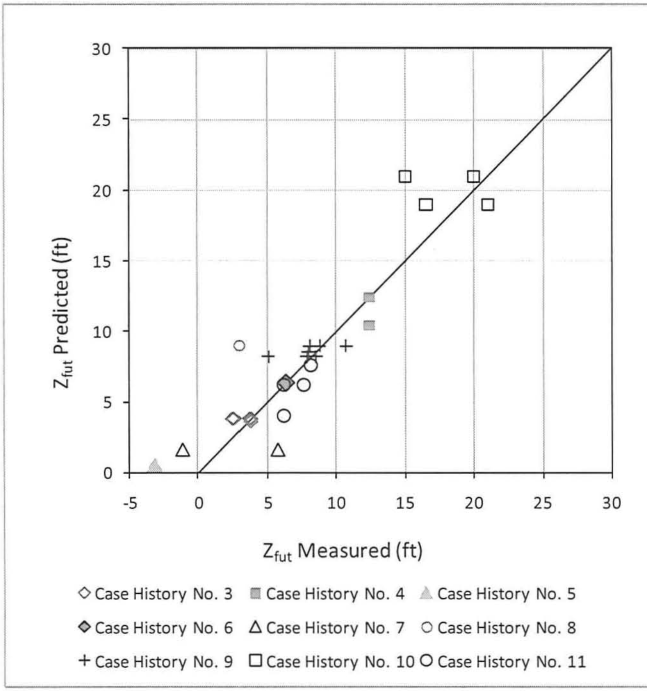

FIGURE 7 BSA 1 validation results.

EXAMPLE APPLICATION OF THE PROPOSED METHOD

Problem: Determine the future scour depth corresponding to the 100-year flood for the following information that characterizes the bridge scour problem:

- Geomaterial type is uniform medium erodibility material (Category III).
- Contraction ratio $R_c = B_2/B_1 = 0.85$, upstream water depth $H_1 = 32.8$ ft (10 m), and pier diameter $D = 3.28$ ft (1.0 m).
- The age of the bridge $t_{hyd} = 25$ years.
- The bridge is not founded in rock.
- The scour conditions are mostly clear-water scour, and a 0.98 ft (0.3 m) infilling is estimated to occur after big floods.
- The maximum observed scour depth $Z_{mo} = 6.56$ ft (2 m).
- The allowable scour depth $Z_{thresh} = 26.3$ ft (8 m).
- The bridge was built in 1981 and assessed in 2006.
- The longitude and latitude of the bridge are –96.0 and 30.0, respectively.

The following is the solution according to BSA 1 flowchart box numbers (Figure 1):

- Box 1-1: Start of BSA 1 (Uniform Deposit). Proceed to Box 1-2.
- Box 1-2: The bridge is not founded in rock. Proceed to Box 1-5.

- Box 1-5: $Z_{mo} = 2$ m; $Z_{thresh} = 8$ m. Proceed to Box 1-6.
- Box 1-6: Infilling is important. Proceed to Box 1-7.
- Box 1-7: Infilling can be quantified.
- Box 1-10: Infilling is estimated at 0.3 m. Proceed to Box 1-11.
- Box 1-11: $Z_{mo} = 2 + 0.3 = 2.3$ m. Proceed to Box 1-12.
- Box 1-12: $Z_{mo} < Z_{thresh}$. Proceed to Box 1-14.
- Box 1-14: To get the velocity ratio $V_{fut}/V_{mo} = V_{100}/V_{mo}$, launch the computer program TAMU-FLOOD and input the following parameters (Figure 8):
  - Input the longitude and latitude of the bridge (–96.0 and 30.0, respectively).
  - Input the year the bridge was built (1981) and the year of the BSA 1 assessment (2006).
  - Choose the Log-Pearson Type III–MOM flood frequency analysis method.
  - Run TAMU-FLOOD. The lower portion of Figure 8 shows the TAMU-FLOOD output, where the maximum recurrence interval of flow at the bridge is 17 years and V_{mo}/V_{100} is between 0.6 and 0.8. Taking V_{mo}/V_{100} as 0.7, $V_{100}/V_{mo} = 1.4$.
- Box 1-15: Medium erodibility material (Category III). Proceed to Box 1-16.
- Box 1-16: From Figure 3(b), $Z_{fut}/Z_{mo} = 1.5$ for a 25-year-old bridge. In this case, $Z_{fut} = Z_{100}$

  $$\begin{aligned} Z_{fut} = Z_{100} &= 1.5 \text{ x } Z_{mo} \\ &= 1.5(7.54 \text{ ft}) = 1.5(2.3 \text{ m}) \\ &= 11.3 \text{ ft } (3.5 \text{ m}) \end{aligned}$$

  Proceed to Box 1-17.
- Box 1-17: The bridge is founded on a uniform soil deposit.
- Box 1-19: $Z_{fut} = Z_{100} = 3.5$ m $= 11.5$ ft; $Z_{thresh} = 8$ m $= 26.2$ ft. Z_{fut} is less than Z_{thresh}. Proceed to Box 1-21.
- Box 1-21: The bridge is deemed "minimal risk" and should undergo regular monitoring. Although the bridge only experienced a 17-year flood event, the results of the analysis predict that it is stable for the predicted 100-year event superimposed on top of the previous flood events. However, if the bridge does experience another major flood, BSA 1 should be carried out again soon after to assess the bridge for a future flood after having undergone the major flood.

It is to be noted here that the software tools TAMU-FLOOD and TAMU-FLOW as well as the Texas Department of Transportation report that describes BSA 1 in detail (Briaud et al. 2009) is available for free download at https://ceprofs.civil.tamu.edu/briaud/simplescour.htm.

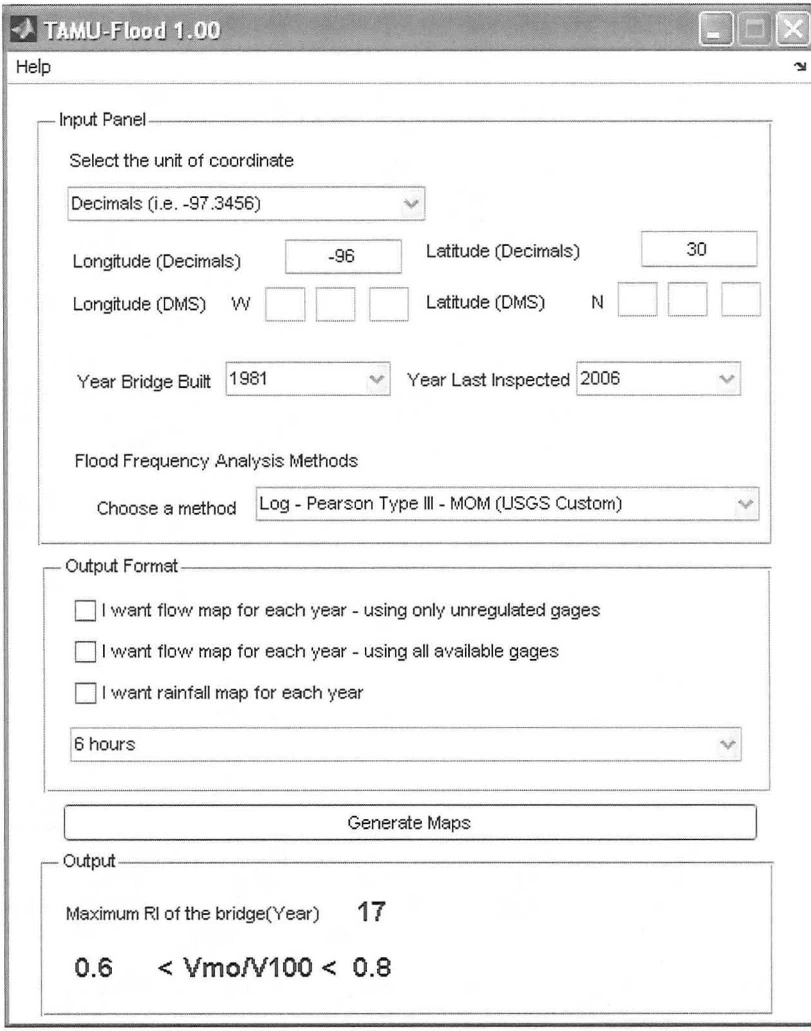

FIGURE 8 TAMU-FLOOD Input and Output for BSA 1 Example.

TABLE 1 Results of the Application of BSA 1 to 16 Bridges in Texas

Application No.	Waterway	Highway	Scour Location	Z_{mo} (ft)	Z_{thresh} (ft)	V_{100}/V_{mo}	Z_{100}/Z_{mo} (from chart)	Z_{100} (ft)	Outcome of BSA 1	Current TxDOT Scour Status
1	Sanders Creek	FM39	Bent 5	1.5	11.3	1.05	1.10	1.7	Stable	Critical
2	Alligator Creek	US287	Bent 3	13.1	16	1.04	1.20	15.7	Stable	Critical
3	Big Creek	SH36	Bent 5	3.8	11	1.00	1.00	3.8	Stable	Critical
4	San Marcos River§	FM2091	Bent 5	12.4	16	0.95	§	§	§	Critical
5	Mill Creek	FM331	Bent 4	0.8	1.5	1.33	1.50	1.2	Stable	Critical
6	Guadalupe River	US87	Bent 27	6.3	8.5	1.11	1.20	7.6	Stable	Critical
7	San Jacinto River	US59SB	Bent 15	5.7	0	1.11	1.20	6.8	Critical	Critical
8	Dry Branch Creek	SH27	Bent 4	9	7.4	1.11	†	†	†	Critical
9	Peach Creek	US59 @ Creekwood Dr.	Bent 2	8.5	17.5	1.20	1.35	11.5	Stable	Critical
			Bent 3	12.1	17.5			16.3		
10	Brazos River	US90A (WB)	Bent 3	21	39	1.67	2.15	45.1	Critical	Critical
11	Navasota River	SH7	Bent 5	8.1	17.5	1.17	1.35	11.0	Stable	Stable
12	North Bosque River	SH 22	Bent 8	5	16	1.43	1.55	7.8	Critical	Critical
			Bent 9	8	12			12.4		
13	San Marcos River	SH 80	Bent 8	7.5	12	0.95	1.00	7.5	Stable	Stable
			Bent 9	10	12.5			10		
14	Sims Bayou	SH 35 NB	Bent 4	4	20	1.11	1.20	4.8	Stable	Stable
15	Bedias Creek	US 75	Bent 26	8	8	1.18	1.30	10.4	Critical	Critical
16	Bedias Creek*	SH 90	*	*	*	*	*	*	*	Stable

Notes:

§ A large caisson was added in 1995 at the scour critical pier. It was not possible to extrapolate Z_{mo} that corresponds to a smaller pier size to obtain Z_{fut} for a larger pier size.

† Z_{mo} exceeds Z_{thresh}. The 9 ft of scour was obtained in 1996. However, the channel backfilled by 6 ft in 1998 and this did not change until 2006.

* Channel excavation was carried out and no corresponding date was indicated in the bridge folder.

APPLICATION OF BSA 1 TO SCOUR CRITICAL BRIDGES

In this study, 16 bridges were selected for application of BSA 1. Of these bridges, 11 were the same ones selected for validation, and 5 were additional bridges selected solely for the application process. TxDOT characterized 12 of the 16 bridges as scour critical and the remaining 4 as stable. Both stable and scour critical bridges were selected to test the proposed bridge scour assessment method and to compare it against TxDOT's scour designation.

For all cases evaluated, the future flow was taken as the 100-year flood with a corresponding velocity, V_{100}. Results of the application of BSA 1 to the 16 bridges are provided in Table 1. The observations of the application procedure are summarizes as follows:

- 6 scour critical bridges were found to be stable by BSA 1
- 3 bridges could not be evaluated using BSA 1 due to reasons explained in the footnotes of Table 1
- 7 bridges had outcomes similar to the TxDOT designation, out of which 3 were stable and 4 were scour critical
- 6 of the 10 bridges that were originally scour critical and had sufficient information were found to be stable after BSA 1 according to the stability criterion.

CONCLUSIONS AND RECOMMENDATIONS

A new bridge scour estimation method termed BSA 1 was proposed. This method was sponsored by TxDOT, finalized in April 2009 and six months later has already been used by TxDOT engineers to evaluate 350 scour critical bridges in the State of Texas. The method overcomes the qualitative nature of current bridge scour evaluations by introducing a formal quantitative framework of a Level 1 analysis. The proposed method is relatively simple, economical and incorporates the field scour behavior of the bridge by using in-situ measurements. It does not require site-specific erosion testing. This paper also introduces a relatively simple and economical method to estimate hydraulic parameters required for scour analysis. The method has been developed for the State of Texas but its framework could be applied to any region having sufficient flow gages. BSA 1 was validated against actual field measurements and the results showed good agreement between measured and predicted values.

BSA 1 was applied to 10 scour critical and 3 non scour critical bridges. As a result of this, 6 of the 10 scour critical bridges were found to be stable and the 3 non scour critical bridges were confirmed as non scour critical. The procedure could introduce huge savings to bridge owners throughout the United States, and quite possibly worldwide.

The following are the authors' recommendations:

- Studies should be carried out to quantify the amount of infilling that takes place in live-bed scour conditions. This could be in the form of scour-monitoring methods or sediment transport analysis.

- The level of risk associated with employing BSA 1 should be studied and addressed. It would be meaningful to determine the probability of the Z_{fut}/Z_{mo} ratios predicted using BSA 1 exceeding field values.
- The time-dependent abutment scour depth should be included in BSA 1 and BSA 3.
- The software tool TAMU-FLOOD should be developed for all the states in the country.

GLOSSARY OF SYMBOLS

- Z_{fut} = scour depth corresponding to a specified future flood
- Z_{mo} = maximum observed scour at the bridge when BSA 1 is performed
- Z_{fut}/Z_{mo} = future scour depth ratio
- V_{fut} = velocity corresponding to the specified future flood
- V_{mo} = maximum velocity observed at the bridge when BSA 1 is performed
- V_{fut}/V_{mo} = future velocity ratio
- Z_{thresh} = allowable scour depth of the foundation
- Z_{infill} = thickness of infill in the scour hole
- H_1 = upstream water depth
- B_1 = uncontracted channel width
- B_2 = contracted channel width
- R_c = contraction ratio = B_2/B_1
- V_c = critical velocity of geomaterial
- D = pier diameter
- t_{hyd} = age of the bridge when BSA 1 is performed
- Z_{max} Ratio = ratio of maximum (equilibrium) future scour depth to Z_{mo}. This is applicable only to Category I and II materials.
- Q_{100} = flow corresponding the 100-year flood
- Q_{mo} = flow value of the maximum flood experienced by the bridge when BSA 1 is performed
- RI_{Qmo} = recurrence interval of Q_{mo}

ACKNOWLEDGEMENTS

This paper is an outcome of a bridge scour project funded by the Texas Department of Transportation (Grant No. 0-5505). The authors are grateful for this support.

REFERENCES

1. Briaud, J.-L., Ting, F.C.K., Chen, H.-C., Gudavalli, R., Perugu, S. and Wei, G. (1999). "SRICOS: Prediction of Scour Rate in Cohesive Soils at Bridge Piers," Journal of Geotechnical and Geoenvironmental Engineering, Vol. 125, No. 4, pp. 237-246.

2. Briaud, J.-L., Ting, F.C.K., Chen, H.-C., Cao, Y., Han, S.W. and Kwak, K.W. (2001a) "Erosion Function Apparatus for Scour Rate Predictions." Journal of Geotechnical and Geoenvironmental Engineering, Vol. 127, No.2, pp. 105-113.

3. Briaud, J.-L., Chen, H.-C., Kwak, K.W., Han, S.W. and Ting, F.C.K. (2001b). "Multiflood and Multilayer Method for Scour Rate Prediction at Bridge Piers," Journal of Geotechnical and Geoenvironmental Engineering, Vol. 127, No. 2, pp. 114-125.

4. Briaud, J.-L., Chen, H.-C., Li, Y., Nurtjahyo, P. and Wang, J. (2005). "SRICOS-EFA Method for Contraction Scour in Cohesive Soils," Journal of Geotechnical and Geoenvironmental Engineering, Vol. 131, No. 10, pp. 1283-1294.

5. Briaud, J.-L. (2008). "Case Histories in Soil and Rock Erosion: Woodrow Wilson Bridge, Brazos River Meander, Normandy Cliffs, and New Orleans Levees - 2007 Ralph B. Peck Lecture," Journal of Geotechnical and Geoenvironmental Engineering, Vol. 134, No. 10, pp. 1425-1447.

6. Briaud J.-L., Govindasamy A.V., Kim, D., Gardoni, P., Olivera, F., Chen, H.-C., Mathewson, C., and Elsbury, K. (2009). "Simplified Method for Estimating Scour at Bridges," Report 0 5505-1, Texas Department of Transportation, Austin, Texas.

7. Cato, K.D. (1991). "Performance of Geologic Materials under Hydraulic Stress," Ph.D. Dissertation, Texas A&M University, College Station, Texas

8. Govindasamy, A.V., Briaud, J.-L., Chen, H.-C., Delphia, J., Elsbury, K., Gardoni, P. Herrman, G., Kim, D., Mathewson, C.C., McClelland, M., and Olivera, F. (2008). "Simplified Method for Estimating Scour at Bridges," GeoCongress 2008, New Orleans, Louisiana, pp. 385-393.

9. Govindasamy, A.V. (2009). "Simplified Method for Estimating Future Scour Depth at Existing Bridges," Ph.D. Dissertation, Texas A&M University, College Station, Texas.

10. Holnbeck, S.R. and Parrett, C. (1997). "Method for rapid estimation of scour at highway bridges based on limited site data," Water-Resources Investigations Report 96-4310, United States Geological Survey, Helena, Montana, pp. 79.

11. Hosking J.R.M and Wallis J.R. (1997). "Regional Frequency Analysis: An Approach based on L-Moments," Cambridge University Press, Cambridge, UK.

12. Huizinga, R.J. and Rydlund, P.H. (2004). "Potential-scour assessments and estimates of scour depth using different techniques at selected bridge sites in Missouri," Scientific Investigations Report 2004-5213, United States Geological Survey and Missouri Department of Transportation, Reston, Virginia, pp. 42.

13. Johnson, P.A. (2005). "Preliminary Assessment and Rating of Stream Channel Stability Near Bridges," Journal of Hydraulic Engineering, Vol. 131, No. 10, pp. 845-852.

14. Lagasse, P.F., Schall, J.D., Johnson, F., Richardson, E.V., and Chang, F. (1995). "Stream Stability at Highway Structures," Federal Highway Administration Report No. FHWA-IP-90-014 (HEC 20), Washington D.C., pp. 144.

15. Pagan-Ortiz, J. E. (1998). "Status of scour evaluation of bridges over waterways in the United States," Proc., ASCE Conf. on Water Resour. Engrg., ASCE, Reston, Va., pp. 2–4.

16. Richardson, E. V. and Davis, S.M. (2001). "Evaluating Scour at Bridges," Publication No. FHWA NHI 01-001 (HEC 18), United States Department of Transportation, Washington, D.C.

17. Simon, A., Outlaw, G.S., and Thoman, R. (1989). "Evaluation, modeling and mapping of potential bridge scour, West Tennessee," Proc., Bridge Scour Symp., Federal Highway Administration and United States Geological Survey, pp. 112-139.

18. Wang, J. (2004). "The SRICOS-EFA method for complex pier and contraction scour," Ph.D. Dissertation, Texas A&M University, College Station, Texas.